

A para-model agent for dynamical systems

Loïc MICHEL

Abstract

Consider a dynamical system $u \mapsto x, \dot{x} = f_{nl}(x, u)$ where f_{nl} is a nonlinear (convex or nonconvex) function, or a combination of nonlinear functions that can eventually switch. We present, in this preliminary work¹, a generalization of the standard model-free control, that can either *control* the dynamical system, given an output reference trajectory, or *optimize* the dynamical system as a derivative-free optimization based "extremum-seeking" procedure. Multiple applications² are presented and the robustness of the proposed method is studied in simulation.

Contents

1	Introduction	1
2	General Principle	1
2.1	Definition of the closed-loop	2
2.2	Definition of the PMA algorithm	2
2.3	Optimization of the performances in simulation	2
3	Applications of the \mathcal{C}_π-control	4
3.1	Control of switched non-minimum and minimum phase systems . . .	4
3.2	Ballistic and the fire control	11
3.3	Control of the HIV-1 model	20
3.4	Control of the Epstein frame	23
4	Derivative-free & "extremum-seeking" control	30
4.1	Proposed \mathcal{C}_π control scheme	30
4.2	Numerical applications	31
5	Concluding remarks	33

¹This work is distributed under CC license <http://creativecommons.org/licenses/by-nc-sa/4.0/>. Email of the corresponding author : loic.michel54@gmail.com

²The control of the Epstein frame (described in §3.4) has been experimentally validated and the results have been presented at the French Symposium of Electrical Engineering in Grenoble, Jun. 2016 <http://sge2016.sciencesconf.org/>.

1 Introduction

Based on the model-free control methodology, originally proposed by [1] [2], which is referred to as a self-tuning controller in [3] and which has been widely successfully applied to many mechanical and electrical processes, the para-model agent (PMA) aims to generalize the model-free control by not only controlling nonlinear system, but also performing an "extremum-seeking" control. On the one hand, we studied the dynamic performances when controlling generic switched minimum phase, non-minimum phase systems (e.g. [4] [5] [6] [7] [8] [9] [10]) as well as the control of some nonlinear systems taken from applications in physics. On the other hand, we present how the PMA can be used to find the optimum of some classes of nonlinear functions. The proposed para-model agent³ is a simple derivation of the discrete model-free control law [13]. The last progresses result in two contributions: first, the substitution of the computation of the numerical derivatives in the original model-free control approach [2], by an initialization function that makes the controller more robust when stabilizing for example switched processes⁴. Then, we propose to extend the properties of the model-free controller to include the extremum seeking control of nonlinear systems without any computation of derivative or gradient. In this case, instead of tracking a working point of nonlinear systems, an appropriate choice of the output reference may stabilize nonlinear systems to their extremum.

The paper is structured as follows. Section 2 presents the general principle of the proposed para-model agent. In Section 3, some examples illustrate the control of generic switched linear systems, the control of a ballistic fire, the control of a biological system and the control of the measure of magnetic hysteresis in the framework of magnetic materials characterization (this last application is also referred to as the control of nonlinear switched systems). Section 4 presents how the proposed PMA approach can be used as derivative-free optimization / "extremum-seeking" control.

2 General Principle

We consider a nonlinear SISO dynamical system to control:

$$u \mapsto y, \quad \begin{cases} \dot{x} = f_{nl}(x, u) \\ y = Cx \end{cases} \quad (1)$$

where f_{nl} is a nonlinear system, the para-model agent is an application $(y^*, y) \mapsto u$ whose purpose is to control the output y of (1) following an output reference y^* .

³A justification of the proposed name "para-model" is given in the note of the conclusion.

⁴The first steps toward the elaboration of the proposed algorithm were to extend the capabilities of the model-free control regarding the control of switched non-minimum phase systems [11].

In simulation, the system 1 is controlled in its "original formulation" without any modification / linearization.

2.1 Definition of the closed-loop

Consider the control scheme depicted in Fig. 1 where \mathcal{C}_π is the proposed PMA controller.

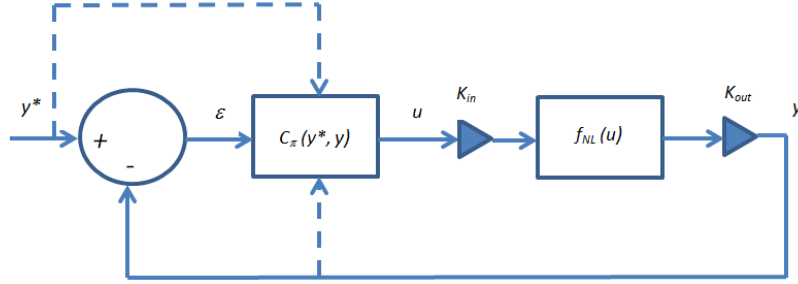


Figure 1: Proposed PMA scheme to *control* or *optimize* a nonlinear system.

2.2 Definition of the PMA algorithm

For any discrete moment t_k , $k \in \mathbb{N}^*$, one defines the discrete controller \mathcal{C}_π such that symbolically:

$$\mathcal{C}_\pi : (y, y^*) \mapsto u_k = \int_0^t K_i \varepsilon_{k-1} d\tau \Big|_{k-1}^{\mathbb{R}^2 \rightarrow \mathbb{R}} \{u_{k-1} + K_p(k_\alpha e^{-k_\beta k} - y_{k-1})\} \quad (2)$$

where: y^* is the output reference trajectory; K_p and K_I are real positive tuning gains; $\varepsilon_{k-1} = y_{k-1}^* - y_{k-1}$ is the tracking error; $k_\alpha e^{-k_\beta k}$ is an initialization function where k_α and k_β are real constants; practically, the integral part is discretized using e.g. the Riemann sums. Thus, we define the set of \mathcal{C}_π -parameters of the controller as the set of coefficients $\{K_i, K_p, k_\alpha, k_\beta\}$.

2.3 Optimization of the performances in simulation

Optimizing the performances in simulation means that we want to solve the problem of finding the most appropriate set of \mathcal{C}_π -parameters relating to the minimization of some performances index ⁵, that may quantify the dynamical performances of the

⁵The classical performance index that are available are IAE, ISE, ITAE, and ITSE. see e.g. (<http://www.mathworks.com/matlabcentral/fileexchange/18674-learning-pid-tuning-iii--performance-index-optimization/content/html/optimalpidtuning.html>) for a quick review (in the context of PID tuning).

closed-loop. This problem is thus equivalent to an optimization problem for which any optimization solver can be *a priori* used. In particular, meta-heuristic solvers or derivative-free optimization solvers are preferred due to the pretty complexity of the closed-loop nonlinear form (in general). We are interested in using the "Brute Force Optimization" (BFO) solver [12] that is very convenient and efficient to use. Figure 2 illustrates a closed-loop first order system, whose the controlled transient has been BFO-optimized in Fig. 3.

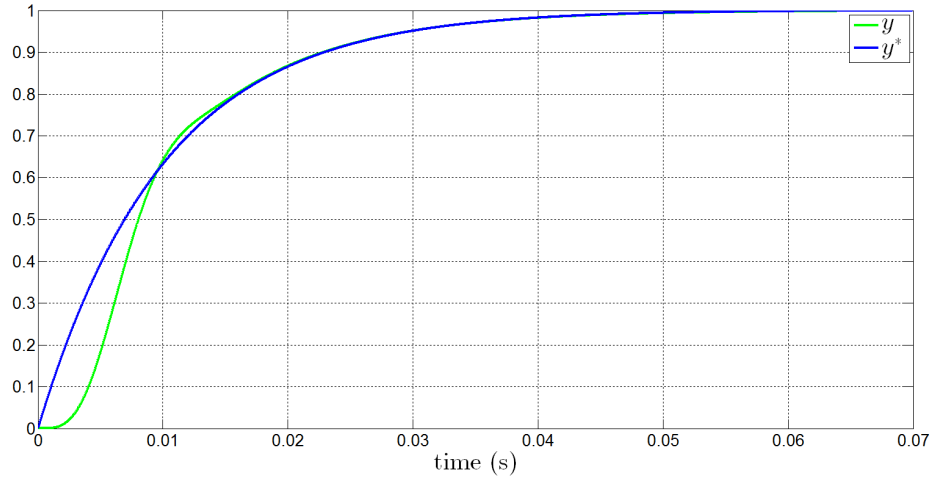


Figure 2: Simulation with a set of \mathcal{C}_π -parameters arbitrary fixed to ensure at least asymptotic stability.

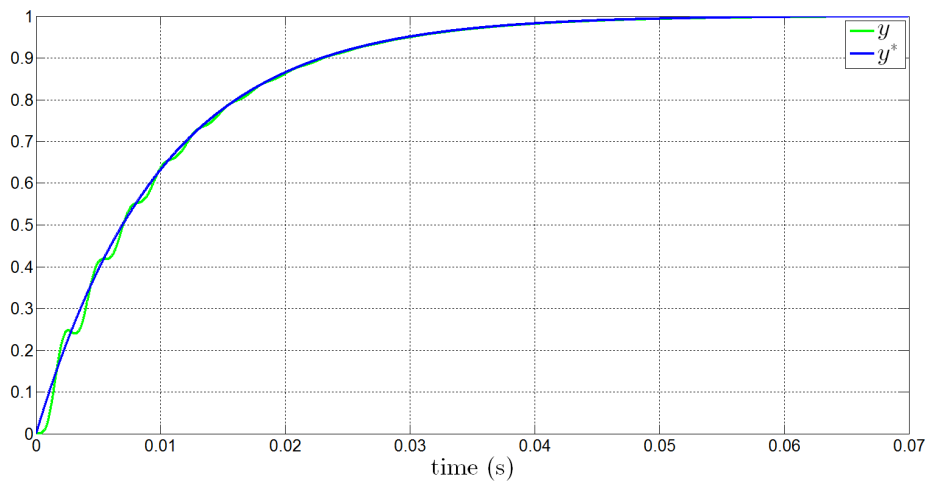


Figure 3: Simulation with a set of \mathcal{C}_π -parameters BFO-optimized to minimize a transient performance index.

3 Applications of the \mathcal{C}_π -control

3.1 Control of switched non-minimum and minimum phase systems

Consider the set Σ of stable linear systems such that $\Sigma = \{\Sigma_i\}, i = 1, 2, \dots, n$, which are minimum and non-minimum phase systems, and which are considered as *unknown* in the sense that no explicit model has been identified for control purposes. Assume now that for all systems, there exists an integer $p = \{1, \dots, 8\}$, called the switching index, such that during a short time window, we have:

$$\Sigma_p(u \mapsto y) := \begin{cases} \dot{x}(t) = A_p x(t) + B_p u(t) \\ y = C_p x(t) \end{cases} \quad (3)$$

where u and y are respectively the input and the output of the system Σ_p (p is the switching index). The step responses of these p systems are presented Fig. 4.

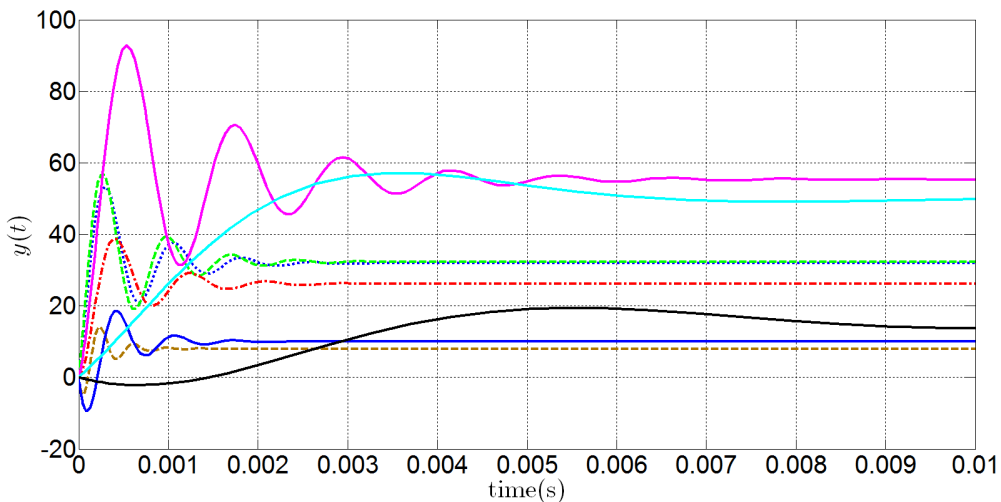


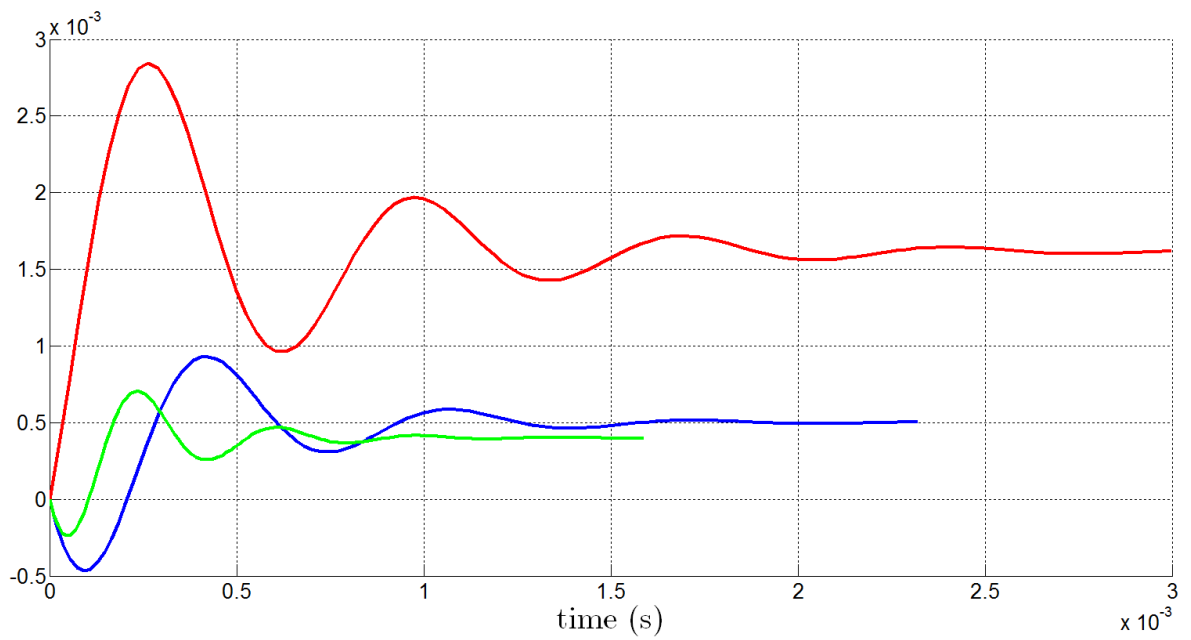
Figure 4: Step responses of each system Σ_i .

Figures 5 6 7 8 present some examples of the application of the \mathcal{C}_π control under different arbitrary switching sequences that involve both minimum and non-minimum phase systems. The first switching time is t_1 , the second is t_2 and the third is t_3 .

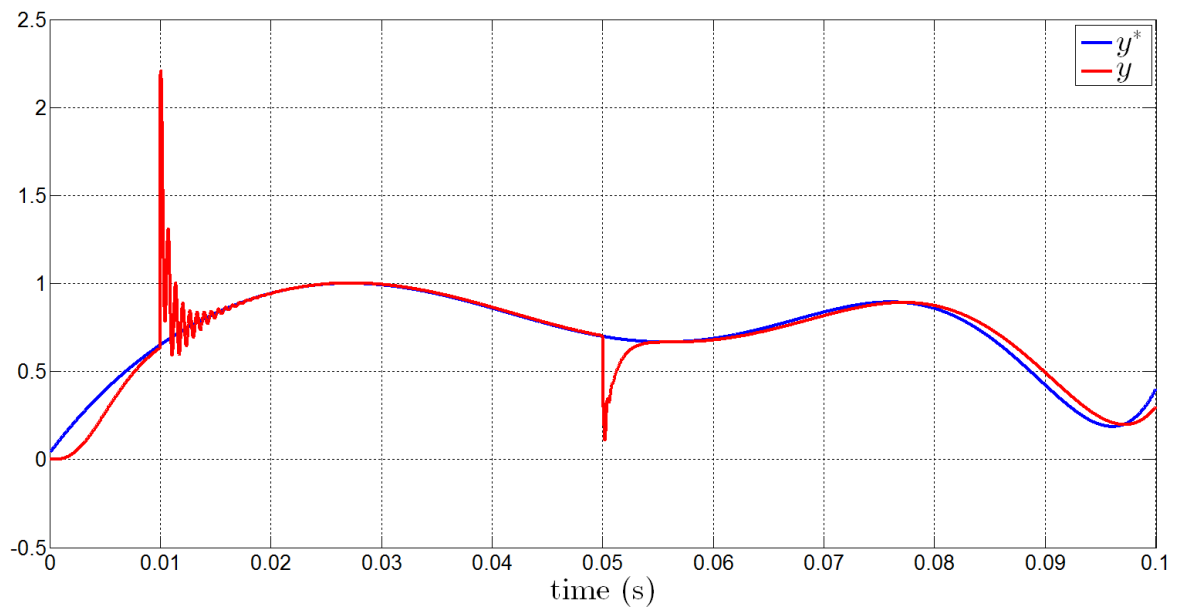
Consider now the existence of a delay τ on y that modify (3) such that:

$$\Sigma_p(u \mapsto y) := \begin{cases} \dot{x}(t) = A_p x(t) + B_p u(t) \\ y = C_p x(t - \tau) \end{cases} \quad (4)$$

This delay can e.g. simulate the propagation delay inside a sensor network. Figures 9 and 10 present two examples of the application of the \mathcal{C}_π control under different switching sequences that involve both minimum and non-minimum phase systems.

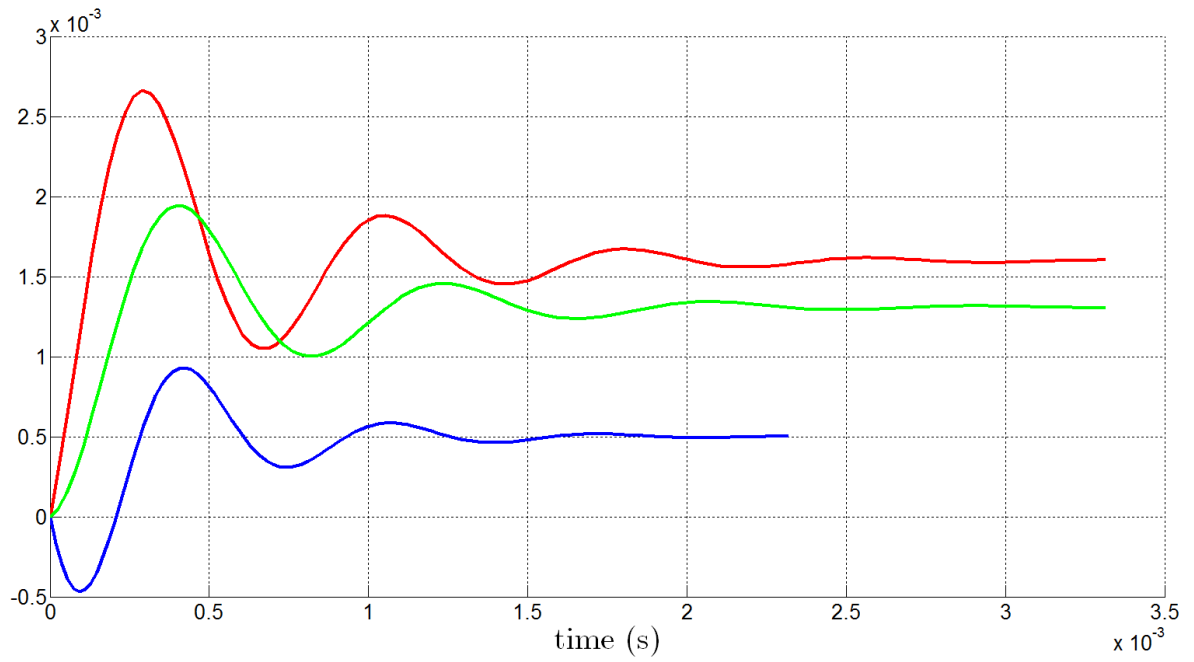


(a) Step responses of each system Σ_i .

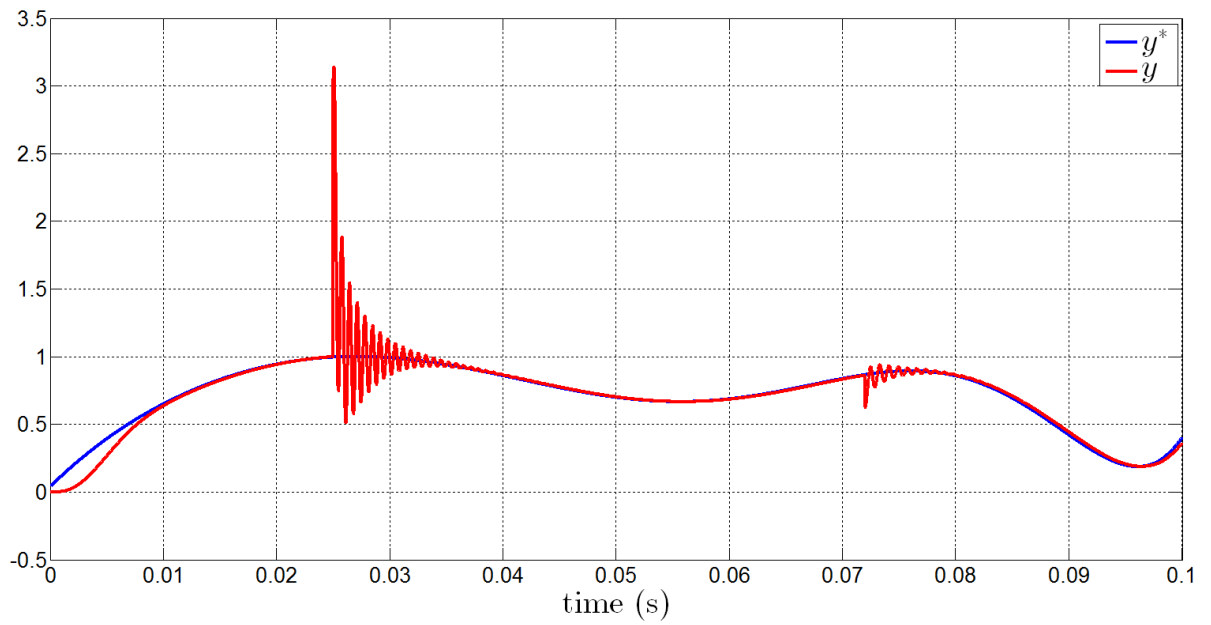


(b) Controlled switched sequence.

Figure 5: Switched sequence #1 for $t_1 = 0.01$ s and $t_2 = 0.05$ s.

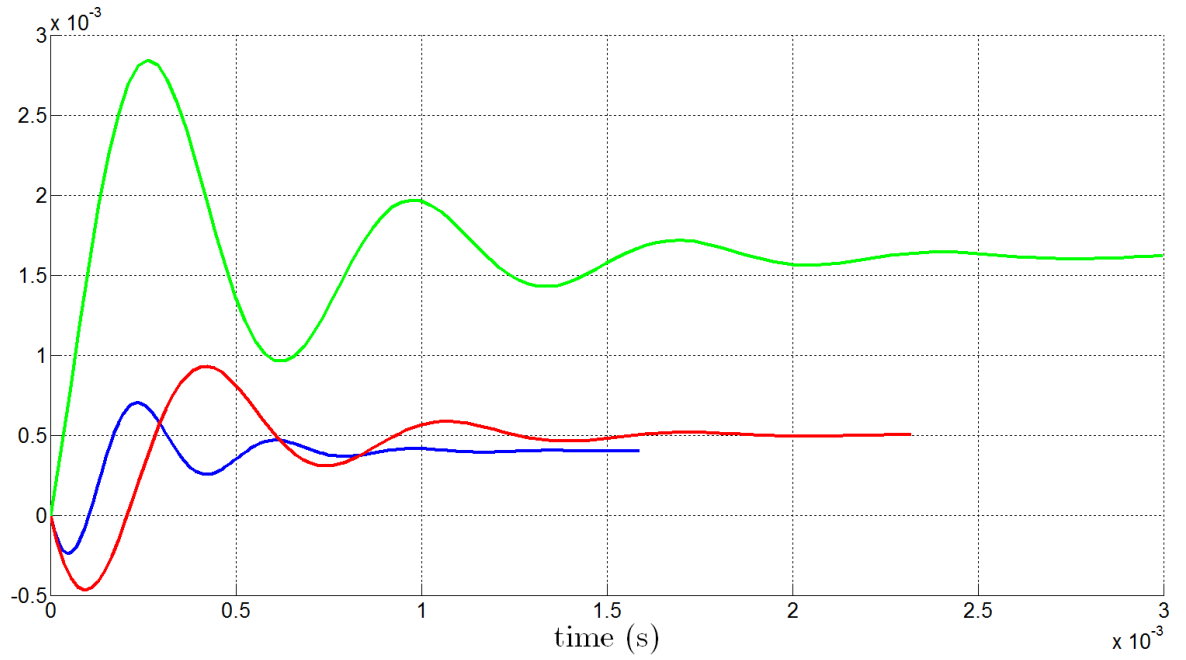


(a) Step responses of each system Σ_i .

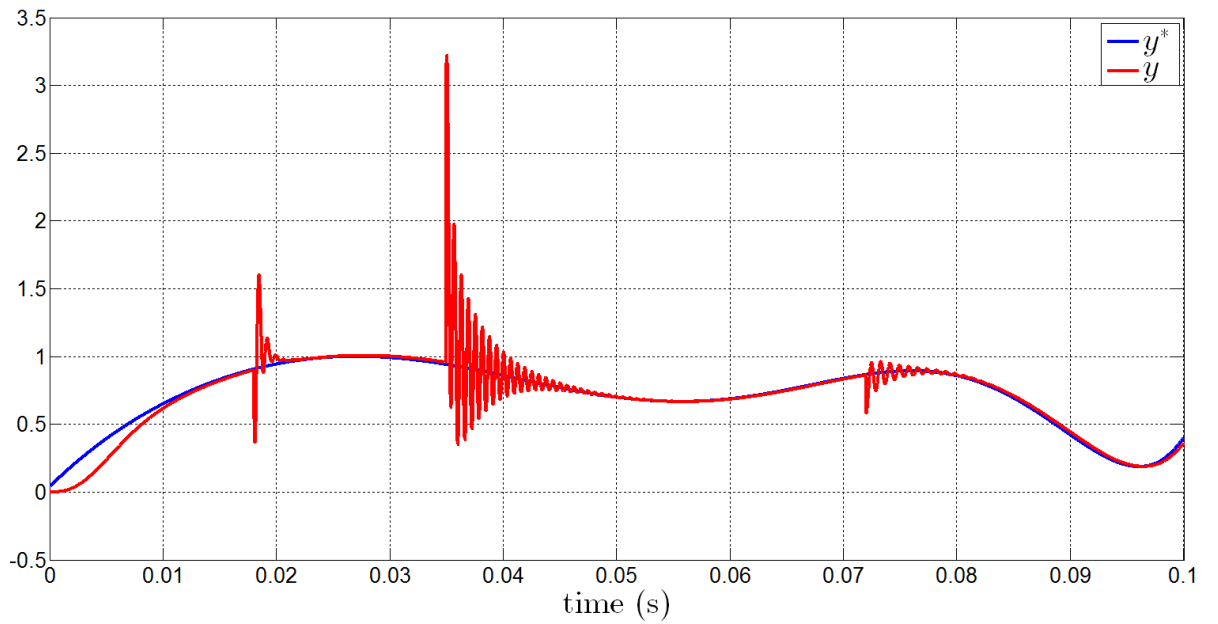


(b) Controlled switched sequence.

Figure 6: Switched sequence #2 for $t_1 = 0.025$ s and $t_2 = 0.072$ s.

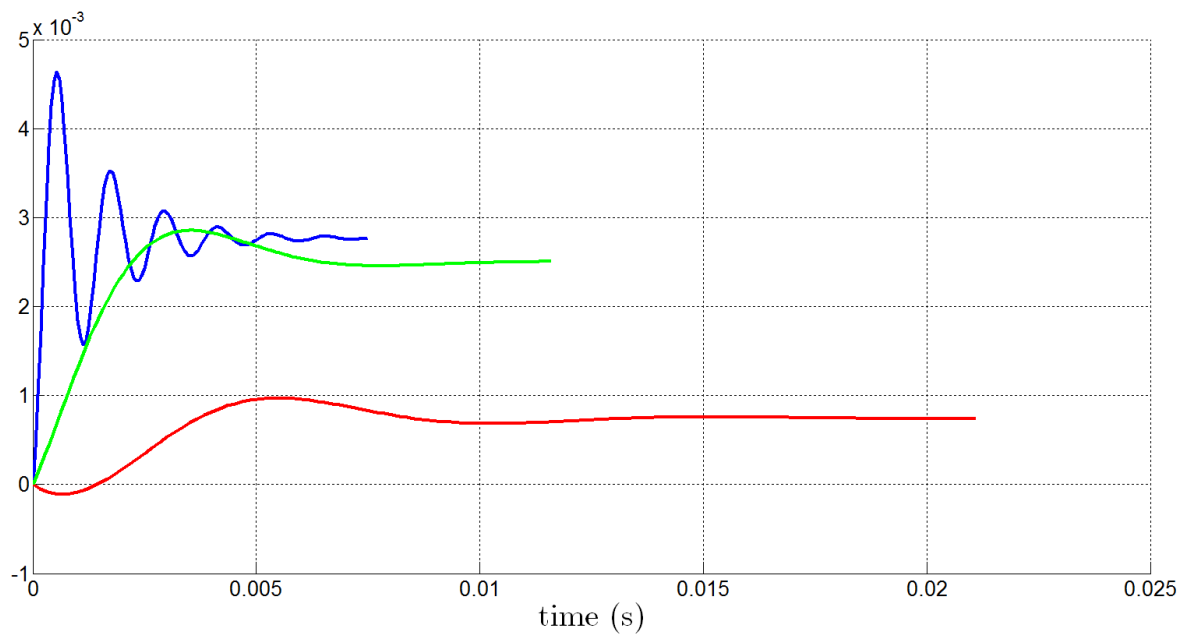


(a) Step responses of each system Σ_i .

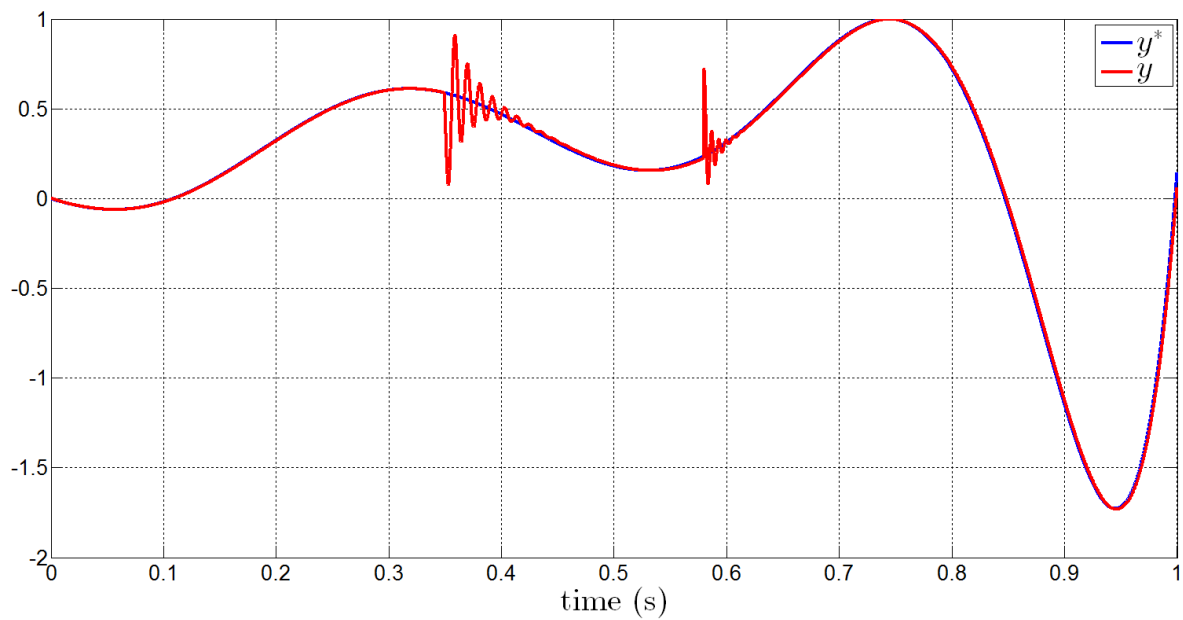


(b) Controlled switched sequence.

Figure 7: Switched sequence #3 for $t_1 = 0.018$ s, $t_2 = 0.035$ s and $t_3 = 0.072$ s.

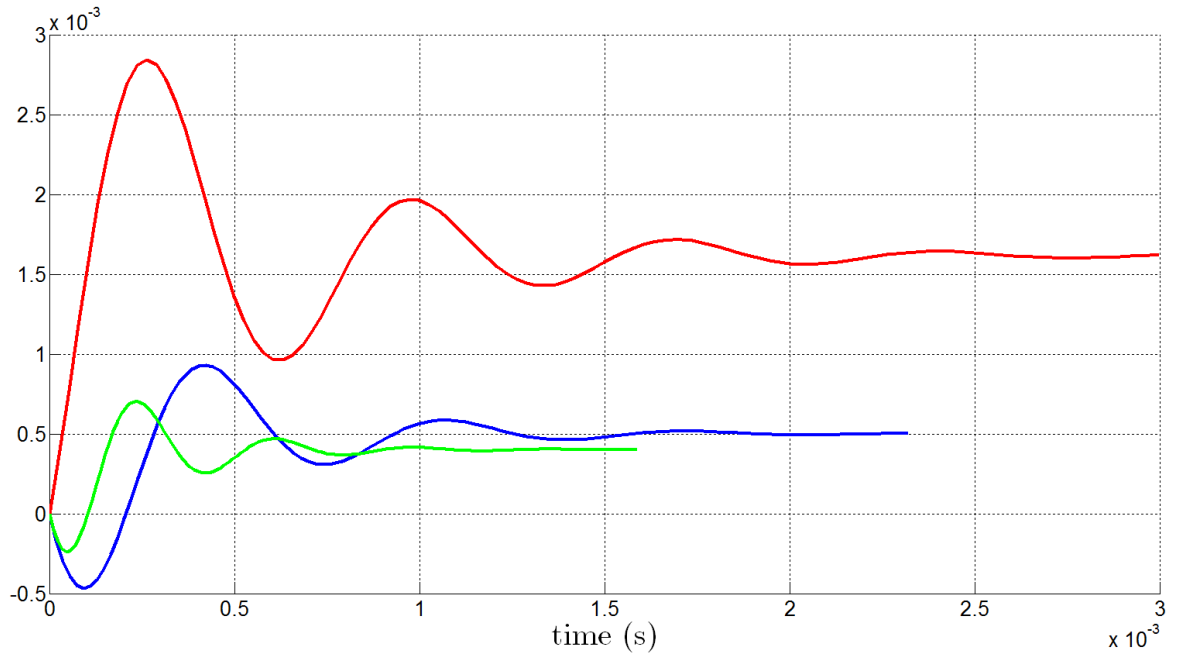


(a) Step responses of each system Σ_i .

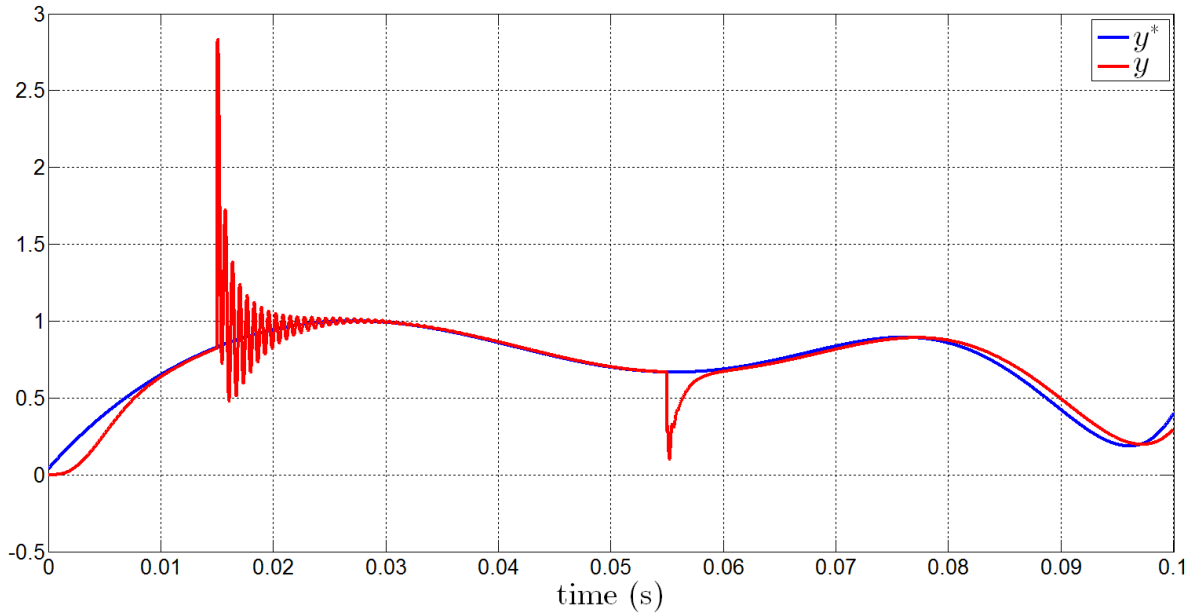


(b) Controlled switched sequence.

Figure 8: Switched sequence #4 for $t_1 = 0.35$ s, $t_2 = 0.58$ s.

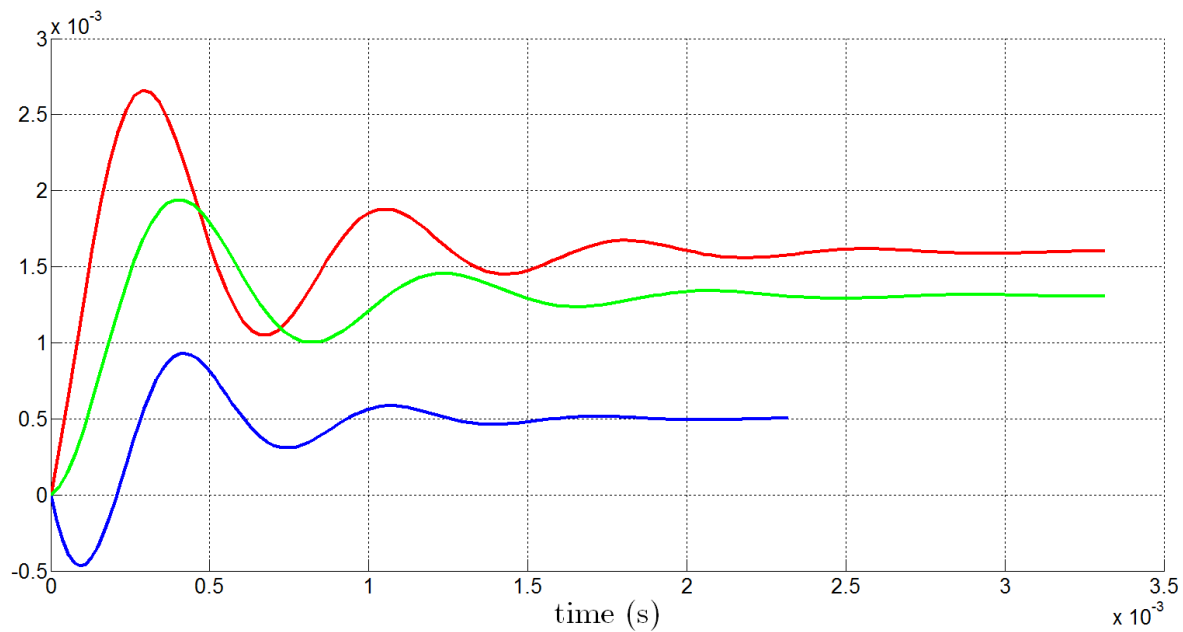


(a) Step responses of each system Σ_i .

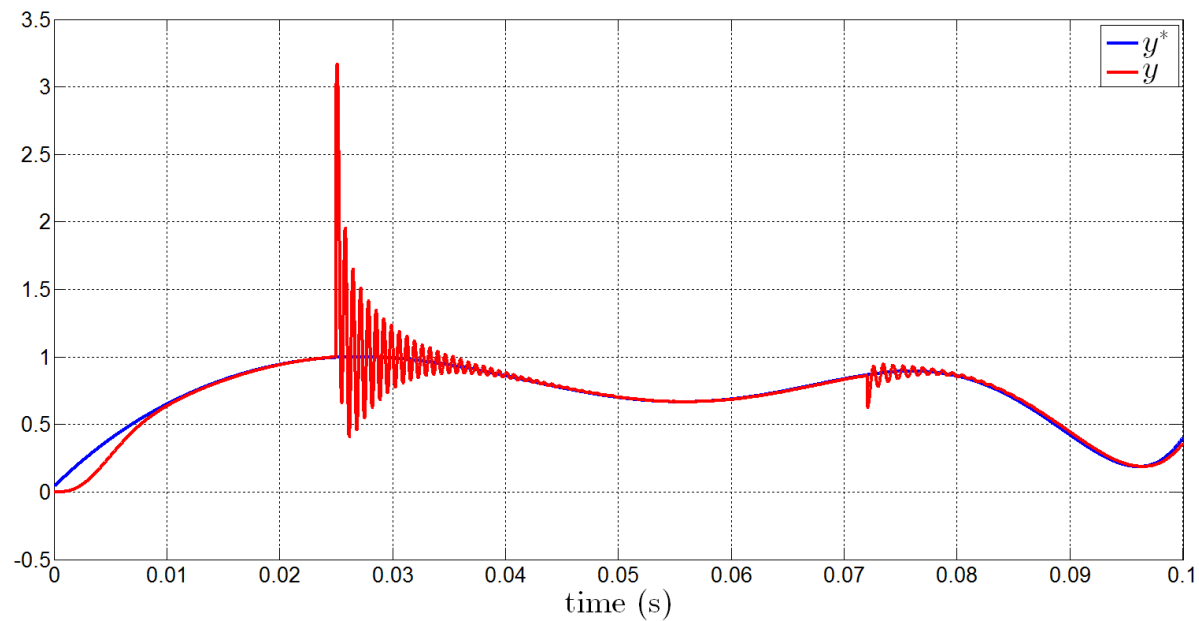


(b) Controlled switched sequence.

Figure 9: Switched sequence #5 for $t_1 = 0.015$ s, $t_2 = 0.055$ s. An addition of a time-delay occurs at $t = 0.06$ s.



(a) Step responses of each system Σ_i .



(b) Controlled switched sequence.

Figure 10: Switched sequence #6 for $t_1 = 0.025$ s, $t_2 = 0.072$ s. An addition of a time-delay occurs at $t = 0.06$ s.

Discussions

These results have been obtained with a single specific set of the \mathcal{C}_π parameters; to improve the tracking performances, one may consider an on-line adjustment of the \mathcal{C}_π parameters. Although resonances occur at the instants of switches, the stability of the control is preserved (regarding the studied cases) when switching from the different types of systems. In the same manner, a direct tuning of the \mathcal{C}_π parameters could damp (ideally, could cancel) the resonant effects.

The presented simulation results show that the proposed control law is robust to "strong" model variations and in particular when the model is a switching non-minimum phase or minimum phase system that include eventually time-delay. Moreover, the proposed control law seems to have the same properties than the original model-free control [1] [2] for which its performances have been successfully verified especially in simulation.

3.2 Ballistic and the fire control

If one fire a projectile at an initial angle and an initial speed, then general physics allows calculating how far it will travel... but would it be possible to *control* the initial speed needed in such manner that the projectile reaches a precise distance? That's what we propose to do using the \mathcal{C}_π -control.

3.2.1 Ballistic simplified model

We define first a simple model of the trajectory $\mathbf{w}(t) = (w_x(t), w_z(t))$ of a projectile of mass m in the usual frame of reference (Oxz) fired with an initial speed magnitude v_0 that makes a fire angle θ with the horizontal reference i.e. $\mathbf{v}(t) = v_0 \cos(\theta)\mathbf{e}_x + v_0 \sin(\theta)\mathbf{e}_z$. The origin $(0, 0)$ of the frame reference is considered as the initial position of the projectile.

Denote \mathbf{a} the acceleration vector and \mathbf{v} the speed vector of the projectile. From Newton law, considering the action of the gravity \mathbf{g} and the air resistance $c\mathbf{v}^2$, we have:

$$m \frac{d^2 \mathbf{w}(t)}{dt^2} = m\mathbf{a} = m\mathbf{g} - c\mathbf{v}^2 \quad (5)$$

with the initial conditions:

$$\left. \frac{dw_x(t)}{dt} \right|_{(0,0)} = v_0 \cos \theta, \quad \left. \frac{dw_z(t)}{dt} \right|_{(0,0)} = v_0 \sin \theta \quad (6)$$

Considering no air resistance i.e. $c = 0$, (5) is simplified:

$$\begin{cases} m \frac{dw_x(t)}{dt} = 0 \\ m \frac{dw_z(t)}{dt} = -mg \end{cases} \quad (7)$$

whose solution reads:

$$\begin{cases} w_x(t) = v_0 \cos \theta t + cte \\ w_z(t) = v_0 \sin \theta t - \frac{1}{2}gt^2 + cte \end{cases} \quad (8)$$

From (8), the range (or the target) of the projectile x_d at $z = 0$ can be easily deduced. We have:

$$d = \frac{2v_0^2 \cos \theta \sin \theta}{g}. \quad (9)$$

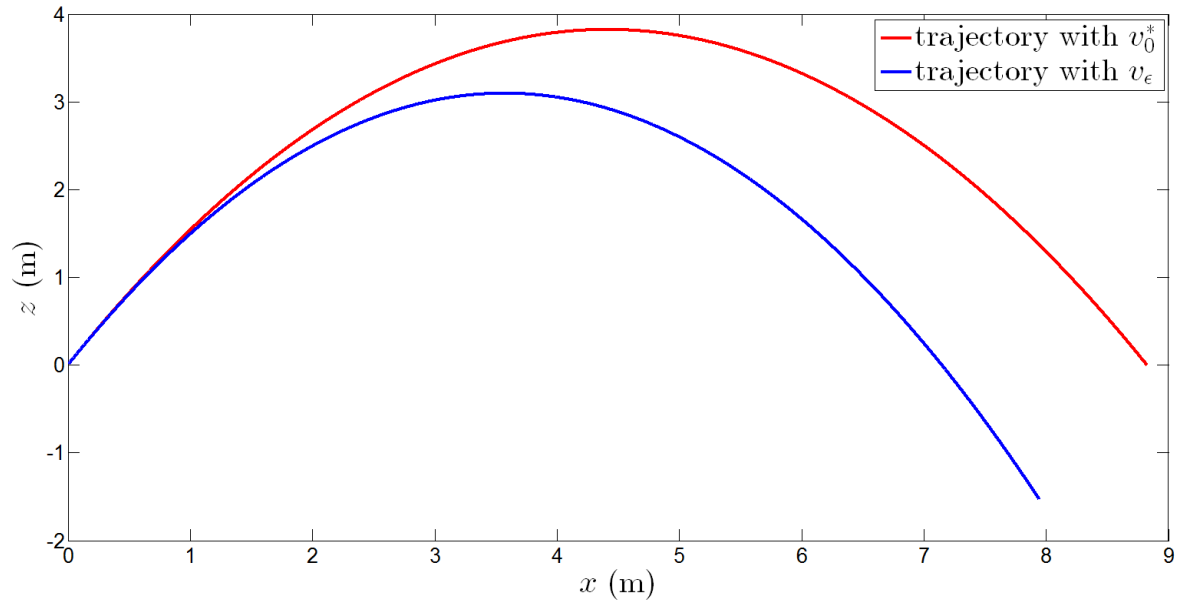
3.2.2 Ballistic-fire control methodology

Proposed strategy Consider by hypothesis that a "virtual" trajectory \mathbf{w}^* of the projectile hits a target x_d^* from an initial speed v_0^* and an initial fire angle θ^* . Consider now the "true" projectile to fire with a trajectory \mathbf{w} . To hit the target x_d^* (at $z = 0$) from a *small initial speed* v_ε , one *controls* the projectile in such manner that the projectile reaches quickly the initial speed v_0^* and the initial fire angle θ^* required to hit the specified target x_d^* according to (9). During such "launching" phase, that we define as the "launching" distance Δx_0 for which the trajectory of the projectile is fully controlled, we start from an initial condition that prevents the projectile to reach its target x_d^* i.e. :

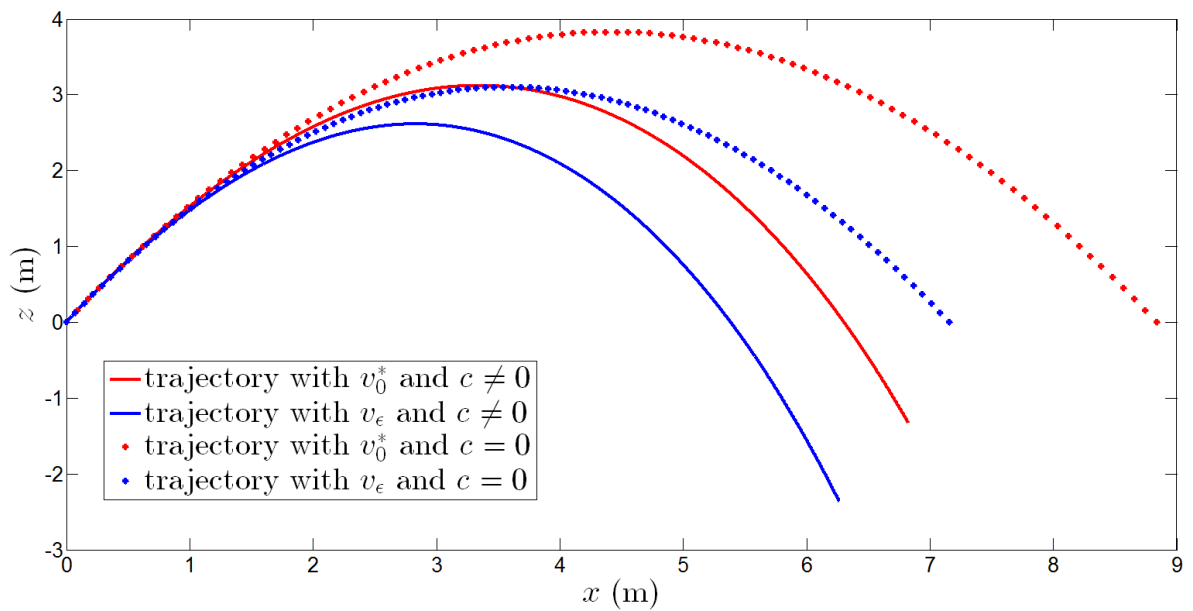
$$\left. \frac{dw_x(t)}{dt} \right|_{(0,0)} = v_\varepsilon \cos \theta_\varepsilon, \quad \left. \frac{dw_z(t)}{dt} \right|_{(0,0)} = v_\varepsilon \sin \theta_\varepsilon \quad (10)$$

where $v_\varepsilon < v_0^*$ and $\theta_\varepsilon \leq \theta^*$ are positive resp. initial speed magnitude and fire angle. Figure 11 illustrates simulation examples of a "virtual" trajectory (subj. to v_0^* and θ^*) and a "true" trajectory (subj. to v_ε and θ^*) that is not controlled; the simulations of the trajectories considering $c \neq 0$ are presented in Fig. 11(b).

The goal is to accelerate the projectile using a specific mechanical device in such manner that the references v_0^* and θ^* are reached quickly. *We consider therefore controlling the trajectory $\mathbf{w}(t)$ of the projectile over the launching distance Δx_0 .*



(a) Case $c = 0$



(b) Case $c = 0$ and $c \neq 0$

Figure 11: Example of comparison of the uncontrolled "true" projectile (subj. to v_ϵ and θ^*) and the "virtual" trajectory (subj. to v_0^* and θ^*), considering $c = 0$ and $c \neq 0$. We took $c = 0.05$, $\theta_\epsilon = \theta^* = \pi/3$, $v_0 = 10$ m/s and $v_\epsilon = 9$ m/s.

Controllable ballistic model

To simulate a controllable model of the trajectory \mathbf{w} of the projectile, we consider adding an external acceleration force in (5) that represents the mechanical action of the specific mechanical device over the distance Δx_0 . We have:

$$m \frac{d^2 \mathbf{w}(t)}{dt^2} = m\mathbf{g} - c\mathbf{v}^2 + \mathbf{a}^{ext} \quad (11)$$

where $\mathbf{a}^{ext}(t) = (a_x^{ext}(t), a_z^{ext}(t))$ is equivalent to the external force provided by the mechanical device. Since such device acts only over Δx_0 , then we assume that $\mathbf{a}^{ext} = \mathbf{0}$ for all $x > \Delta x_0$.

3.2.3 Implementation of the \mathcal{C}_π controller

A possible control scheme is to consider controlling the trajectory \mathbf{w} that must be "as close as possible" to the reference \mathbf{w}^* over the distance Δx_0 . Therefore, \mathbf{w} is physically measured and the external acceleration \mathbf{a}^{ext} is driven by the \mathcal{C}_π controller, through the specific mechanical device.

We build a closed-loop that creates a feedback between (2) and (11). We have "symbolically", for all $x \leq \Delta x_0$:

$$\left\{ \begin{array}{l} \mathbf{u}_k = \mathbf{a}_k^{ext} = \int_0^t K_i(\mathbf{w}_{k-1}^* - \mathbf{w}_{k-1})d\tau \Big|_{k-1} \{ \mathbf{u}_{k-1} + K_p(\alpha e^{-\beta k} - \mathbf{w}_{k-1}) \} \\ m \frac{d^2 \mathbf{w}(t)}{dt^2} = m\mathbf{g} - c\mathbf{v}^2 + \mathbf{u}_k \end{array} \right. \quad (12)$$

Determination of the distance Δx_0^*

Since we expect that the projectile is fired from Δx_0 with a speed that is very close to v_0^* (and follows, via the \mathcal{C}_π control, the same trajectory i.e. $w \approx w^*$ over Δx_0), then, we propose a possible definition of the theoretical launching distance Δx_0^* , (considered only over the x axis) that corresponds to the solution in w_x of:

$$\frac{dw_x(t)}{dt} = v_{0x}^* \quad (13)$$

Geometrically, the theoretical launching distance Δx_0^* is associated to the speed v_x that is reached by the projectile (launched with the initial speed $v_\varepsilon < v_0^*$) when v_x is close to v_{0x}^* .

3.2.4 Numerical simulations

Case $\Delta \mathbf{x}_0 > \Delta \mathbf{x}_0^*$

Consider the simulated "virtual" trajectory, presented in Fig. 11, as the control reference w^* ; to simplify, we consider θ as constant. Figure 12 presents the case where the fire is controlled considering $c = 0$ over $\Delta x_0 = 0.11$ m. In particular, Fig. 12(a) presents, at the top, the evolution of the controlled trajectory w in comparison with the reference w^* , and, at the bottom, the calculated speed dw_x/dt in comparison with the initial speed $v_0 \cos \theta$. Figure 12(b) presents the complete "true" controlled trajectory in comparison with the virtual trajectory. Figure 13 presents the same simulations in the case $c \neq 0$.

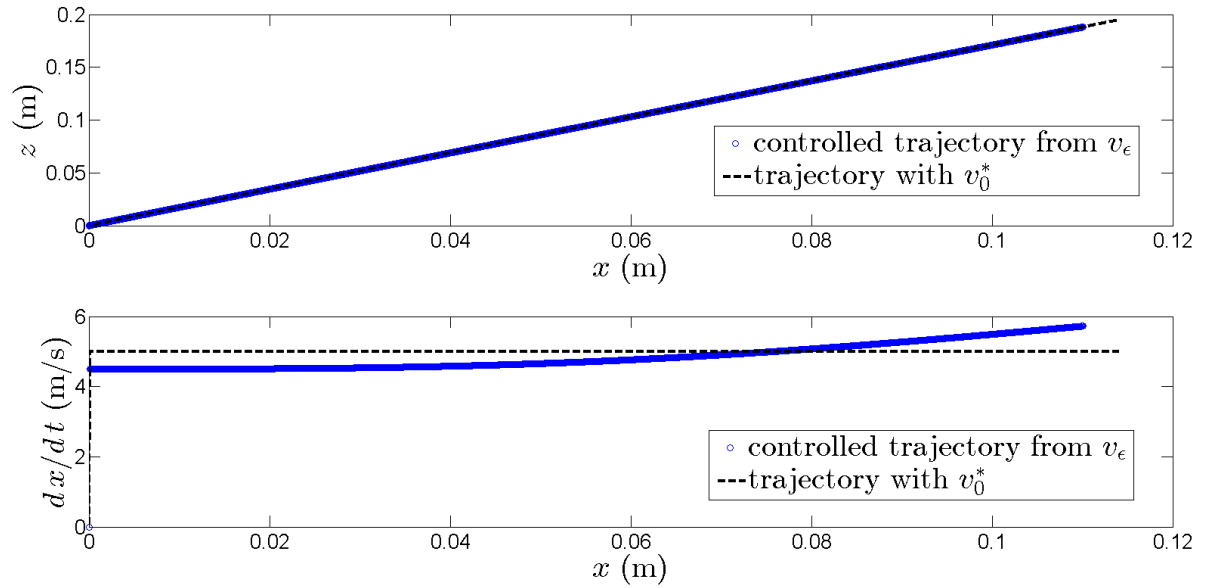
Case $\Delta \mathbf{x}_0 \sim \Delta \mathbf{x}_0^*$

Consider the simulated "virtual" trajectory, presented in Fig. 11, as the control reference w^* ; to simplify, we consider θ as constant. Figure 14 presents the case where the fire is controlled considering $c = 0$ over Δx_0^* . In particular, Fig. 14(a) presents, at the top, the evolution of the controlled trajectory w in comparison with the reference w^* , and, at the bottom, the calculated speed dw_x/dt in comparison with the initial speed $v_0 \cos \theta$. Figure 14(b) presents the complete "true" controlled trajectory in comparison with the virtual trajectory. Figure 15 presents the same simulations in the case $c \neq 0$.

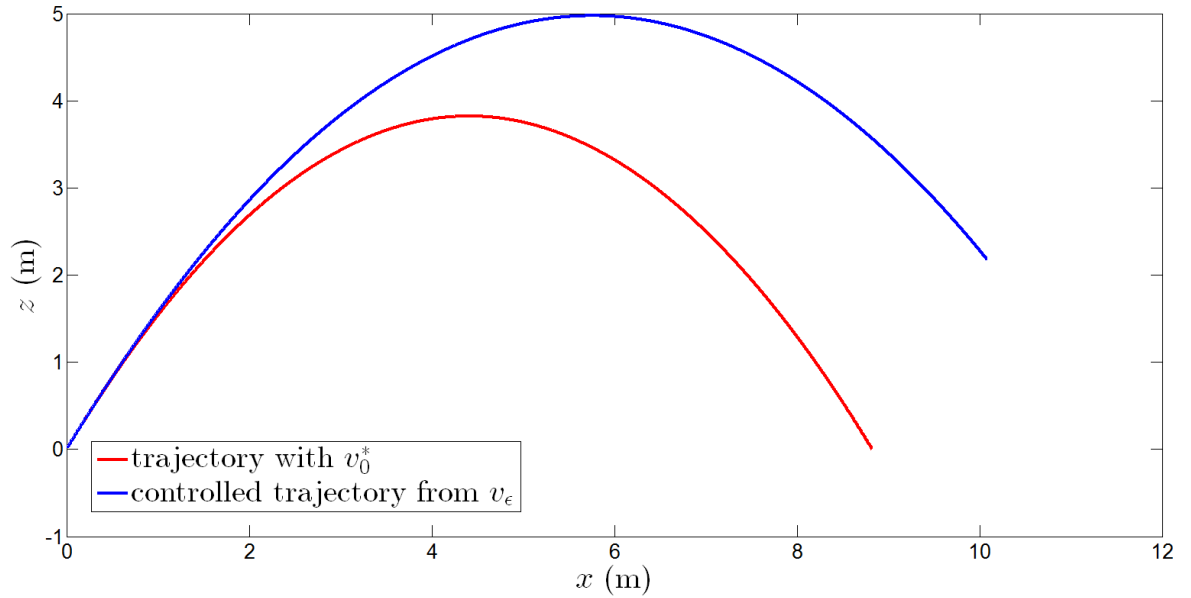
Discussions

These results have been obtained using the same set of the \mathcal{C}_π parameters. The properties of stabilization of the control law, like in the previous case when dealing with switching systems (§3.1), seem to be preserved and ensure good tracking performances in particular when considering $c = 0$ and $c \neq 0$.

Further generalizations would allow using multiple and parallel \mathcal{C}_π controllers in order to control simultaneous physical quantities. In particular, the speed profile \mathbf{v} could be controlled simultaneously with the trajectory \mathbf{w} ...

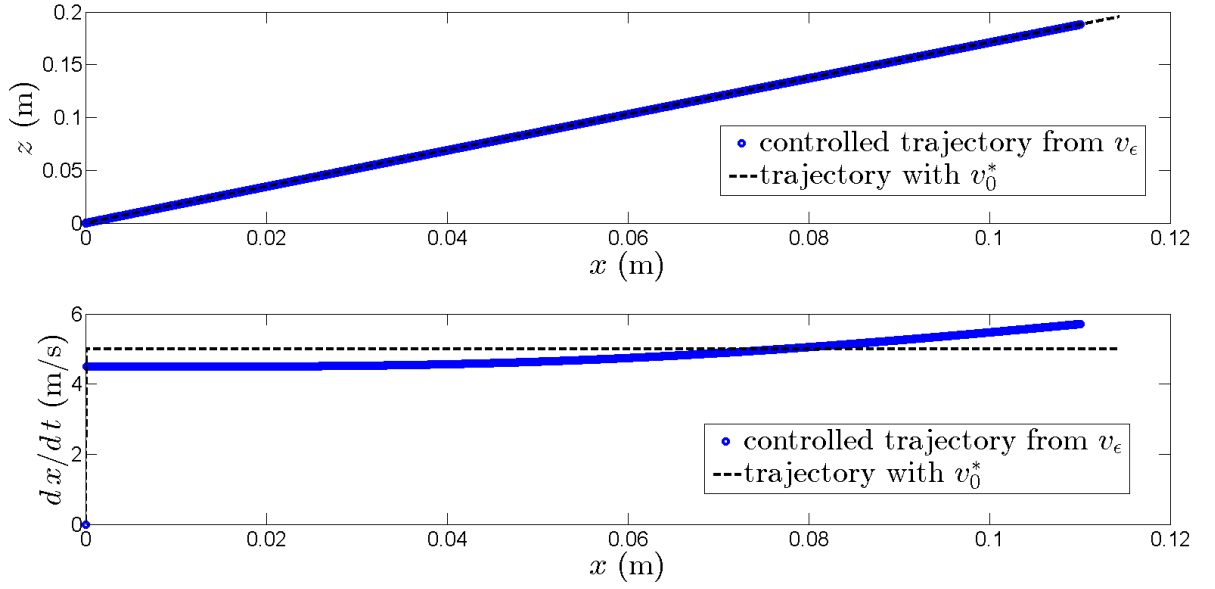


(a) At the top, controlled trajectory w relating to the reference w^* ; at the bottom, calculated speed dw_x/dt relating to the initial speed $v_0 \cos \theta$.

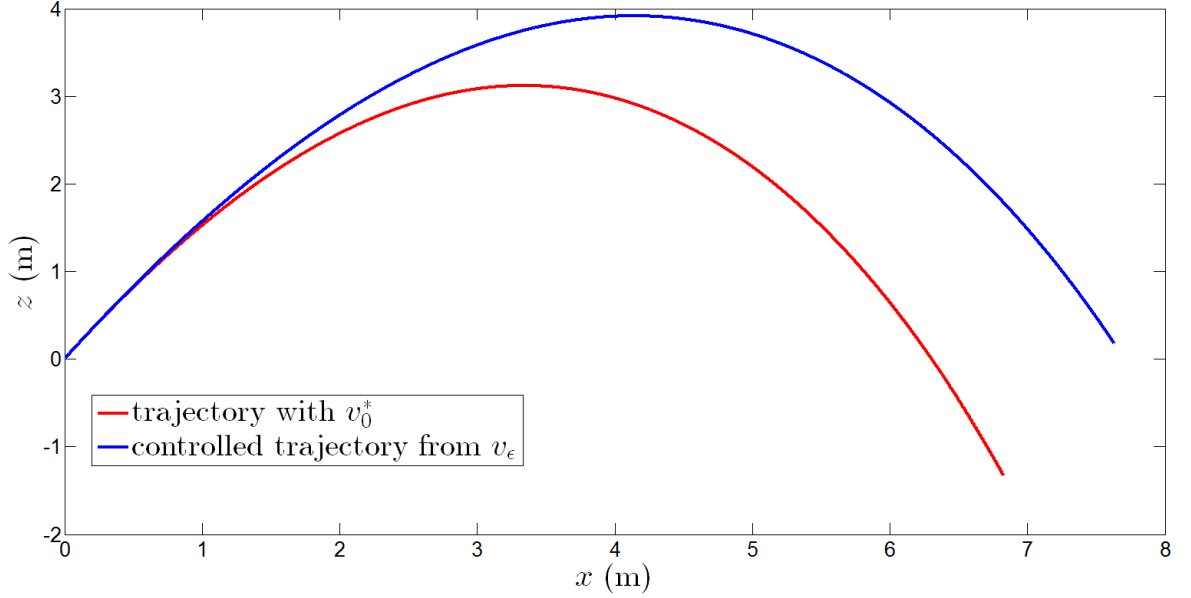


(b) Complete controlled "true" trajectory in comparison with the virtual trajectory.

Figure 12: Example of controlled trajectory considering $c = 0$ over $\Delta x_0 = 0.11$ m. We took $\theta_\epsilon = \theta^* = \pi/3$, $v_0 = 10$ m/s and $v_\epsilon = 9$ m/s.

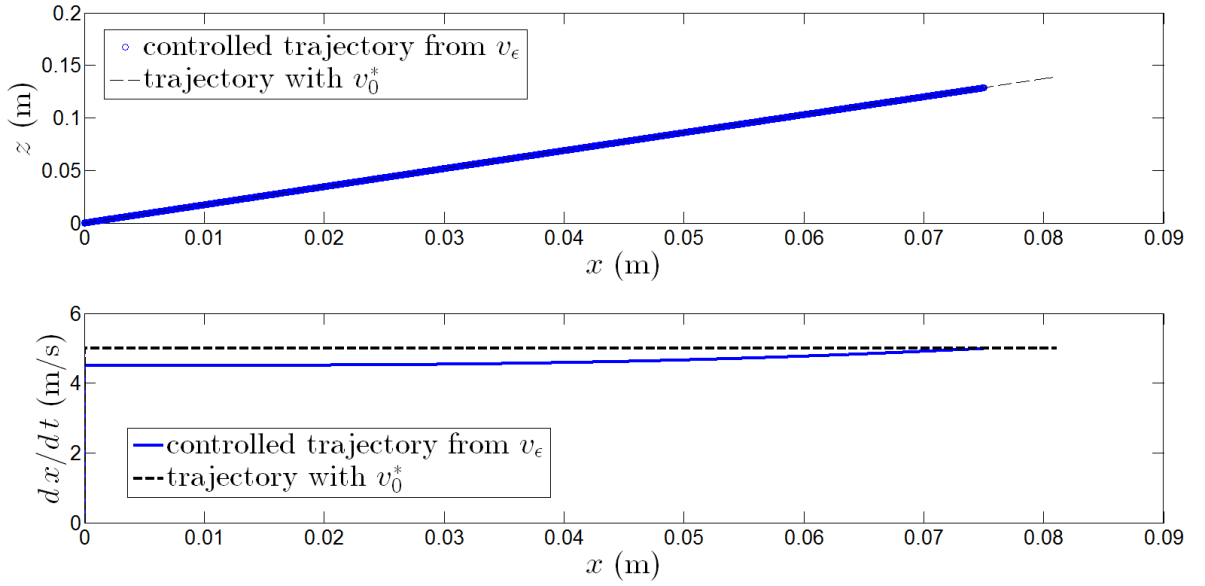


(a) At the top, controlled trajectory w relating to the reference w^* ; at the bottom, calculated speed dw_x/dt relating to the initial speed $v_0 \cos \theta$.

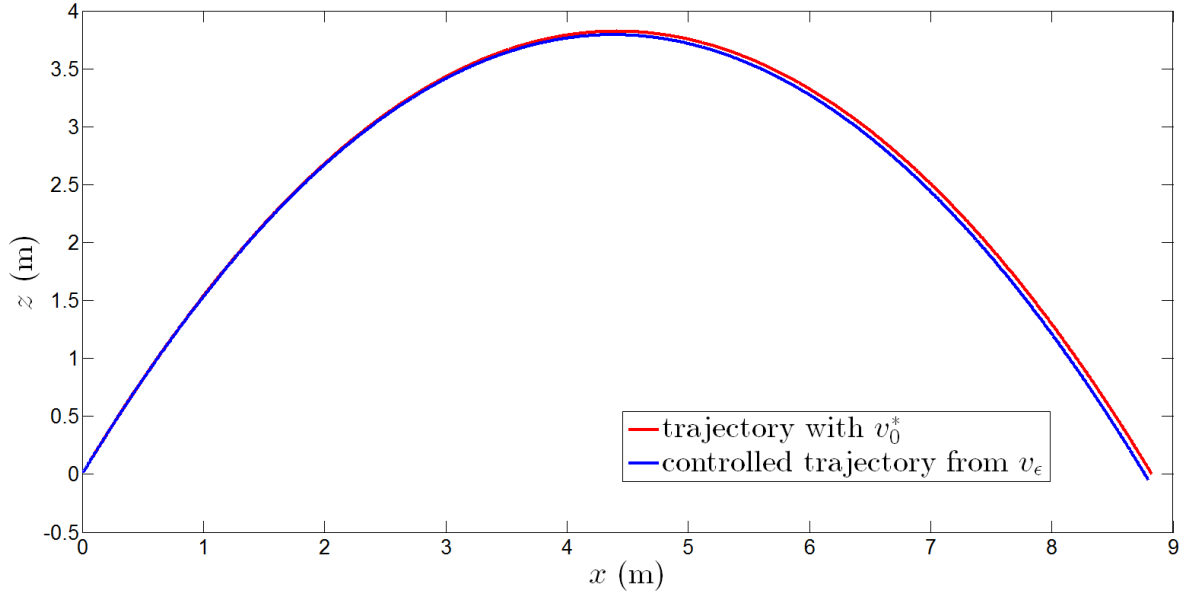


(b) Complete controlled "true" trajectory in comparison with the virtual trajectory.

Figure 13: Example of controlled trajectory considering $c \neq 0$ over $\Delta x_0 = 0.11$ m. We took $c = 0.05$, $\theta_\epsilon = \theta^* = \pi/3$, $v_0 = 10$ m/s and $v_\epsilon = 9$ m/s.

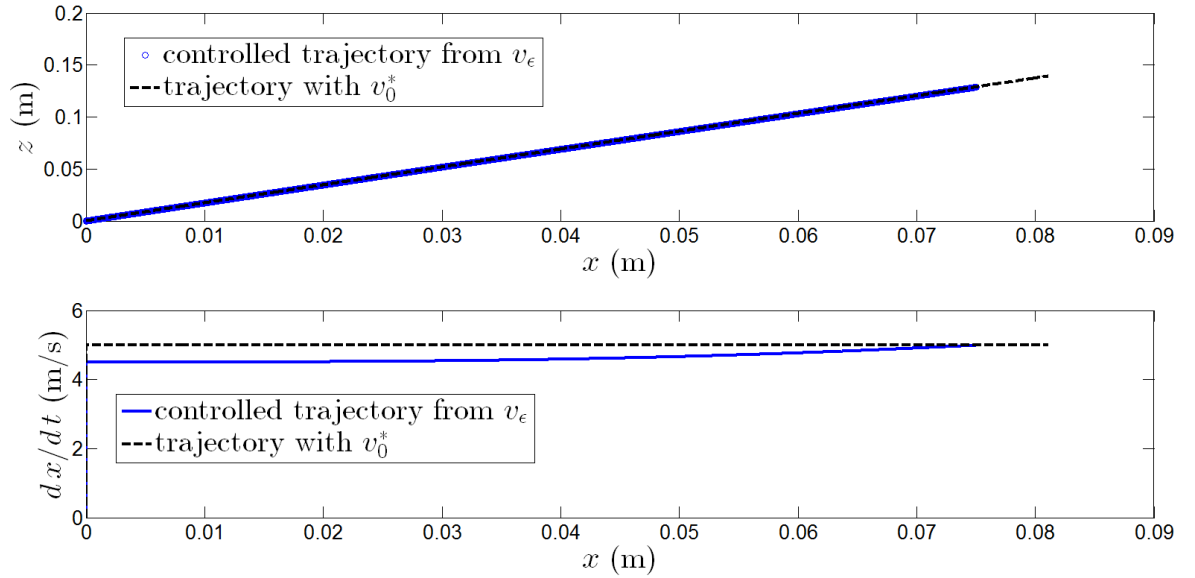


(a) At the top, controlled trajectory w relating to the reference w^* ; at the bottom, calculated speed dw_x/dt relating to the initial speed $v_0 \cos \theta$.

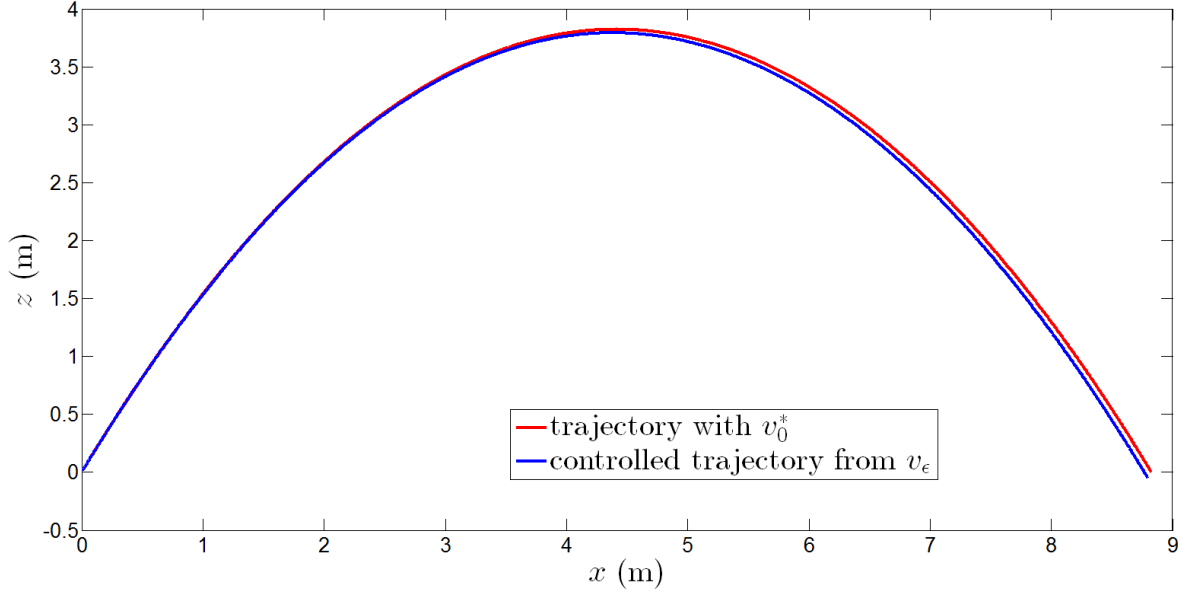


(b) Complete controlled "true" trajectory in comparison with the virtual trajectory.

Figure 14: Example of controlled trajectory considering $c = 0$ over Δx_0^* . We took $\theta_\epsilon = \theta^* = \pi/3$, $v_0 = 10$ m/s and $v_\epsilon = 9$ m/s.



(a) At the top, controlled trajectory w relating to the reference w^* ; at the bottom, calculated speed dx/dt relating to the initial speed $v_0 \cos \theta$.



(b) Complete controlled "true" trajectory in comparison with the virtual trajectory.

Figure 15: Example of controlled trajectory considering $c \neq 0$ over Δx_0^* . We took $c = 0.05$, $\theta_\varepsilon = \theta^* = \pi/3$, $v_0 = 10$ m/s and $v_\varepsilon = 9$ m/s.

3.3 Control of the HIV-1 model

The problem is to control the predator-prey like model that describes the evolution of the HIV-1 when subjected to an external "medical agent". From a mathematical point of view, we study the possibility of controlling the model (14) for which the purpose is to control the output y (corresponding to the viral load) using the double inputs u_1 and u_2 in such manner that y converges rapidly to zero ⁶ [14] [15].

$$\begin{cases} \dot{x}_1 = s - dx_1 - (1 - u_1)\beta x_1 x_3 \\ \dot{x}_2 = (1 - u_1)\beta x_1 x_3 - \mu x_2 \\ \dot{x}_3 = (1 - u_2)kx_2 - cx_3 \\ y = \begin{pmatrix} 0 & 0 & \gamma \end{pmatrix} x \end{cases} \quad (14)$$

where (mathematically) : $d = 0.02, k = 100, s = 10, \beta = 2.4 \cdot 10^{-5}, \mu = 0.24, c = 2.4$. γ is a scaling factor that allows normalizing the output. Figure 16 presents the evolution of the output y in open-loop when $u_1 = u_2 = 0$ i.e. when no medical drug is considered. Figures 17 and 18 illustrate the control of y considering two different ratios between u_1 and u_2 .

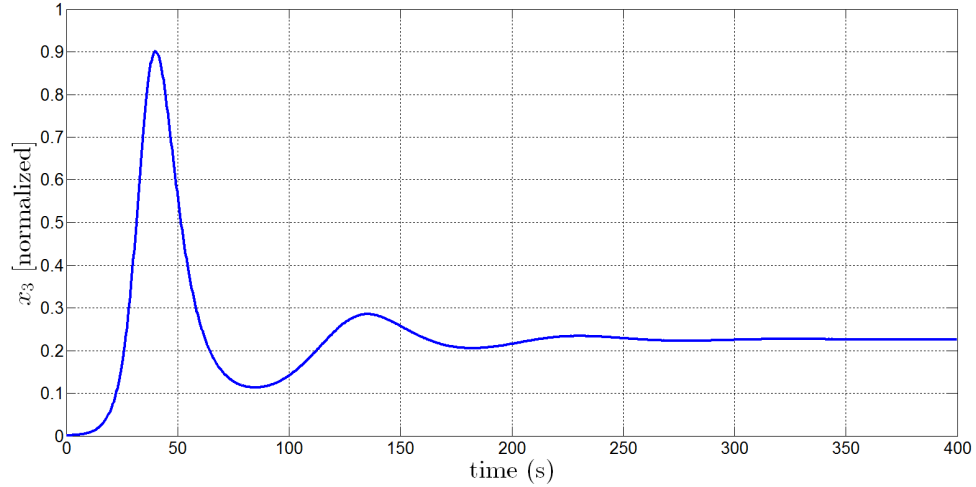
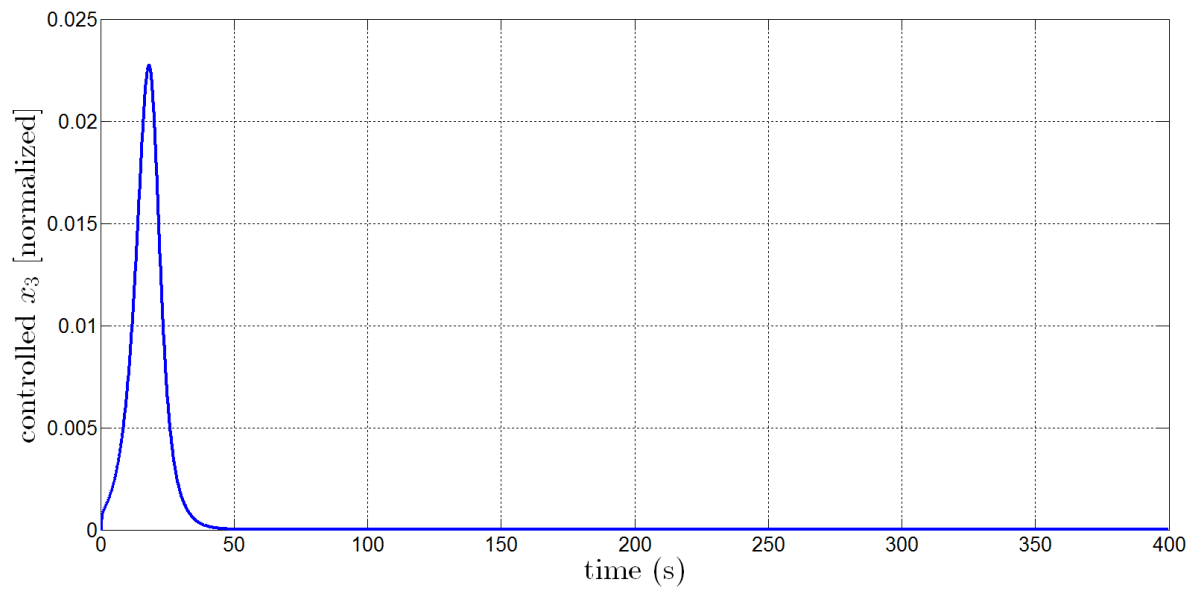
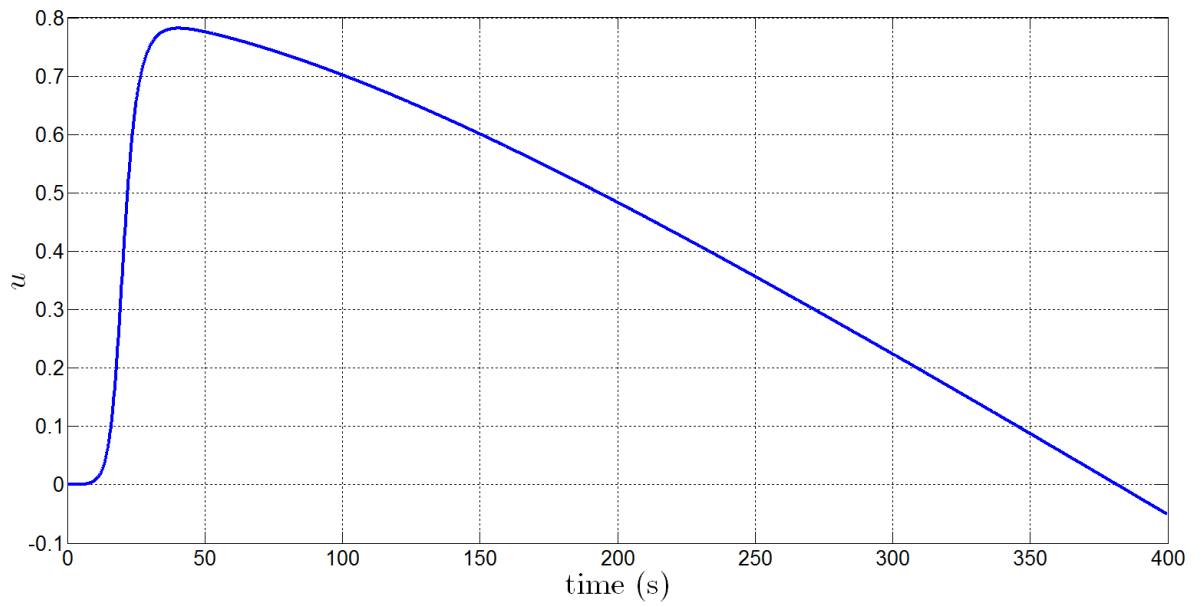


Figure 16: Transient response of y considering $u_1 = u_2 = 0$.

⁶Since we are trying to control this model only from the mathematical point of view, we do not take into account the constraints that are medically imposed.

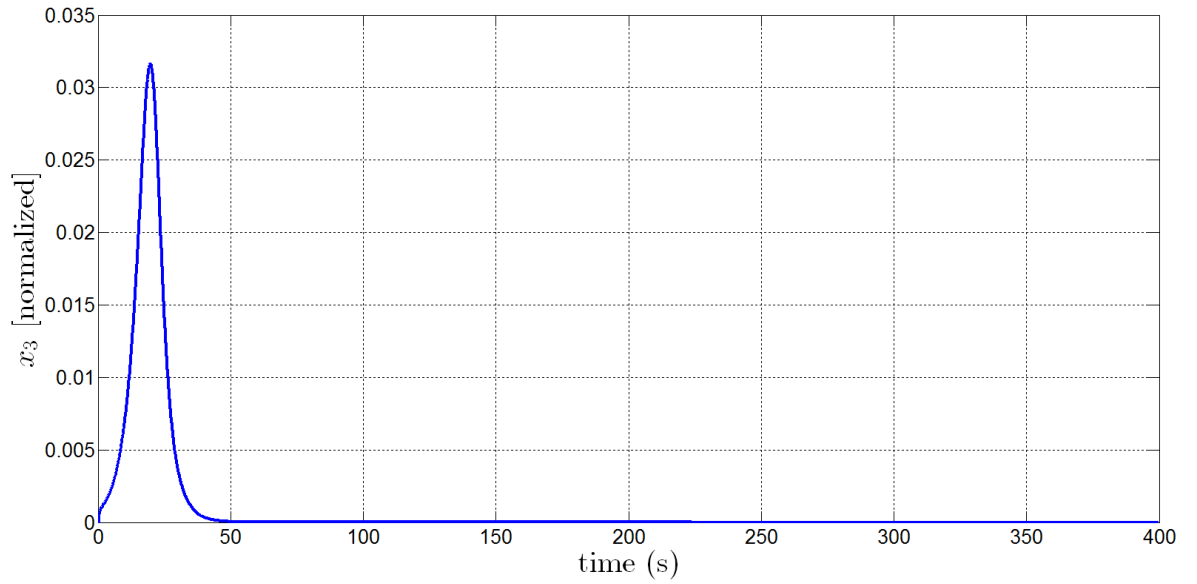


(a) Output y

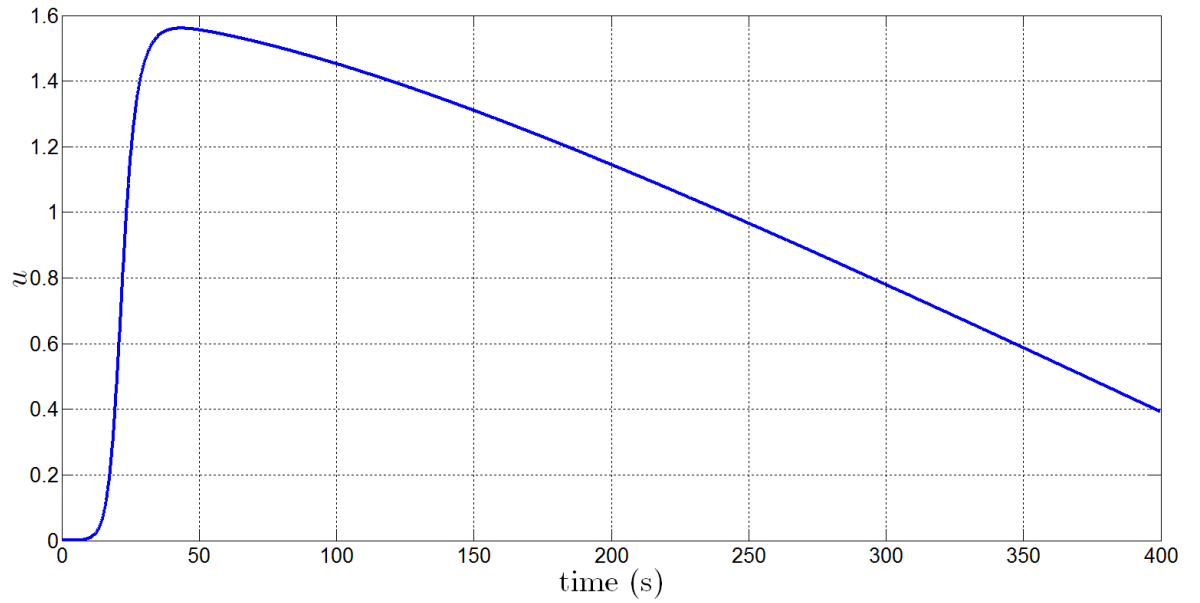


(b) Input u

Figure 17: Controlled output y (viral load) in correspondence with $u_1 = u_2 = u$.



(a) Output y



(b) Input u

Figure 18: Controlled output y (viral load) in correspondence with $u_1 = u_2 = \frac{1}{2}u$.

3.4 Control of the Epstein frame

The Epstein frame (see Fig. 19 ⁷) aims to characterize a magnetic material by determining its $B - H$ hysteresis curve. The principle is to create a *magnetic field* H inside the material using a "magnetizing" current i_H . The material gives a response to the field H that physically corresponds to the measurable *magnetic induction field* B . This B field creates a voltage v_B through magnetic induction and the quantities v_B and i_H is a representation of the magnetic hysteresis curve $B - H$. To describe experimentally the major $B - H$ hysteresis loop, the material under study has to be magnetized using a current i_H that is alternative and of enough magnitude in order to describe the magnetic behavior at saturation. *The purpose of the control law implementation is to control i_H such that the output voltage of the Epstein frame v_B remains "as close as possible" to a desired reference waveform.*

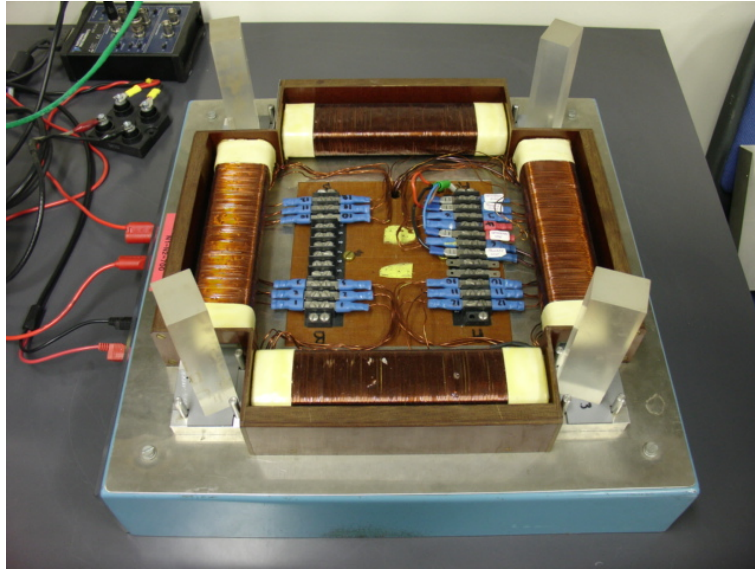


Figure 19: An experimental Epstein frame to characterize magnetic materials.

3.4.1 Epstein frame control

Proposed C_π control scheme Consider the control scheme depicted in Fig. 20 where C_π is the proposed PMA controller. K_{in} and K_{out} are positive real gains. Denote f_{BH} the numerical Jiles-Atherton model that is associated to the magnetic hysteresis $B - H$ and f_{JA} is the complete hysteresis to control.

⁷Picture taken from Wikipedia http://upload.wikimedia.org/wikipedia/commons/5/51/Epstein_frame.jpg.

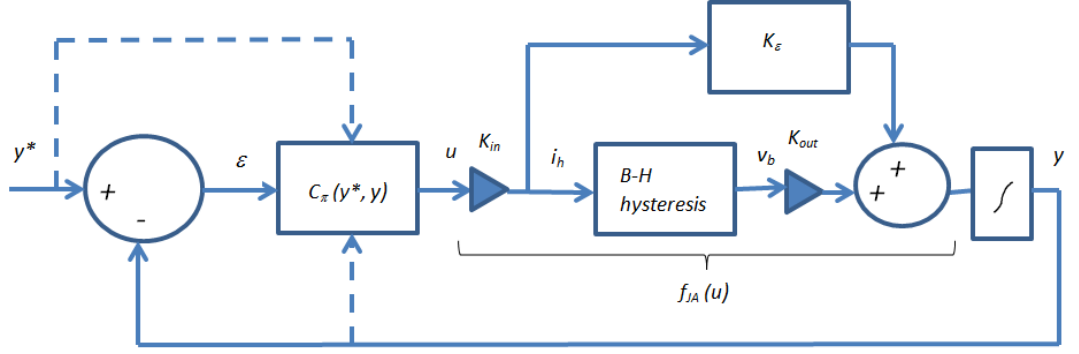


Figure 20: Proposed PMA scheme to control the electrical waveforms measured from a magnetic hysteresis.

Jiles-Atherton based hysteresis model The Jiles-Atherton model [16] describes a magnetic hysteresis cycle $B - H$. It reads:

$$\frac{dM}{dH} = \frac{1}{1 + c\delta k - \alpha(M_{an} - M)} + \frac{c}{1 + c} \frac{dM_{an}}{dH} \quad (15)$$

where c , δk , M_{an} , α are physical coefficients well identified from magnetic hysteresis measurement and we assume that the current i_H corresponds to the magnetization H i.e. $i_H \propto H$ and the voltage v_B corresponds to the derivative of the magnetic induction field response $B = \mu_0 H + J_{BH}(H)$ (where J_{BH} describes the $B - H$ hysteresis via (15)).

Simplified model of the Epstein frame The Epstein frame admits a complex model based on the Jiles-Atherton model that represents all electric phenomena that occur inside the Epstein frame⁸. To simplify the model of the Epstein frame to control, we consider controlling a nonlinear function f_{JA} , which represents a modified Jiles-Atherton model. Denote $v_H = f_{JA}(i_H)$ the nonlinear dynamical system that describes the $B - H$ hysteresis as a function of i_H , and consider controlling directly the hysteresis cycle in such manner that \mathcal{C}_π controls i_H in order to get $v_H = f_{JA}(i_H)$ as close as possible to a reference waveform.

To define the global f_{JA} hysteresis function that is controlled by \mathcal{C}_π , which includes the scaling coefficients needed by the \mathcal{C}_π corrector, consider $i_H = K_{in} u$, $y = K_{out} v_H$ and a coefficient K_e such that:

$$y = f_{JA}(u) = K_{in} K_e u + K_{out} J_{BH}(K_{in} u). \quad (16)$$

⁸The Epstein frame is equivalent to a transformer and the "mutual interactions" between primary and secondary coils must be taken into account in addition to the hysteresis behavior.

The small coefficient $K_e \# 10^{-4}$ compensates the very small variations of f_{BH} when B is close to B_{sat} . Such variations may induce time-delays in the response of the \mathcal{C}_π controller that induce some distortions of the output signal y . The model (16) could be seen as an "affixe" derivation of the original Jiles-Atherton model.

The $B - H$ loops, obtained from the Jiles-Atherton model, are depicted in Fig. 21 considering the frequencies 5 Hz, 50 Hz, 500 Hz, 1 kHz and 10 kHz. Since this hysteresis model does not allow $H > H_{max}$, a limitation is necessary to bound the evolution of H , that may occur eventually during the transient of the dynamic stabilization of the control loop (ex. in Fig. 25).

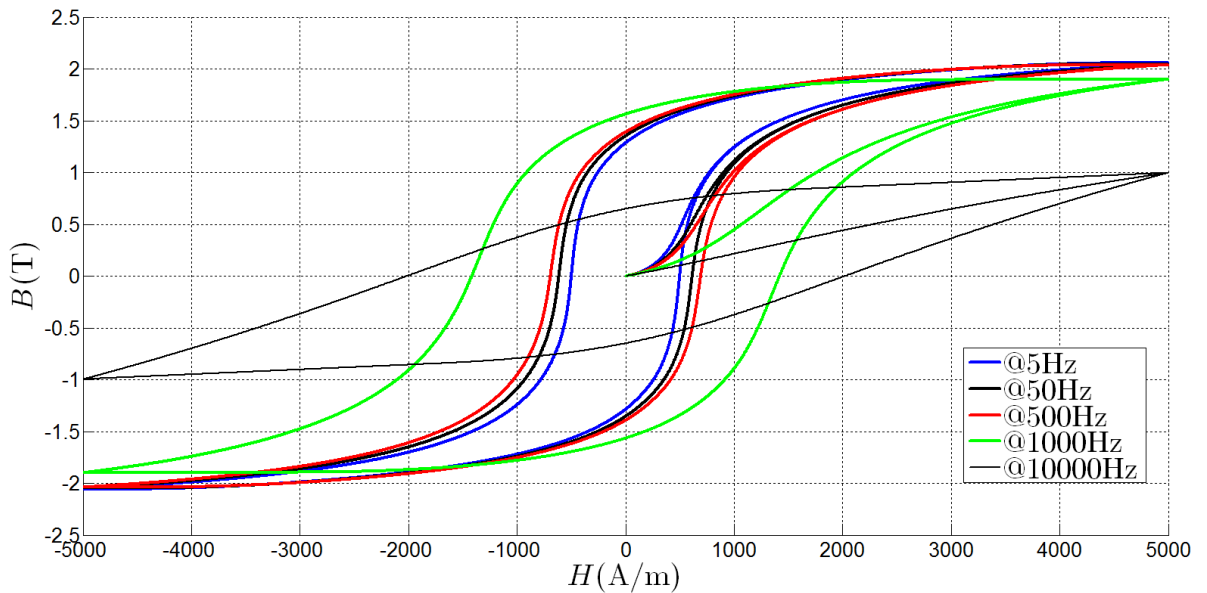


Figure 21: Simulation of the Jiles-Atherton model for different operating frequencies.

3.4.2 Simulation results

Figures 22, 23, 24, 25 and 26 depict the input u and the (rescaled) output y of the control loop according to the time. Given a particular operating frequency, for which a particular $H - B$ hysteresis is studied (see Fig. 21), and assuming that the output reference y^* is a sinusoid, whose magnitude corresponds to the theoretical H_{max} of the $H - B$ hysteresis, different frequencies are considered (5 Hz, 50 Hz, 500 Hz, 1 kHz and 10 kHz) in order to highlight the behavior of the controlled voltage v_b when the frequency changes. In particular, high frequencies (e.g. Figures 25 and 26) introduce an important transient response on y due to the fact that the variations of y^* are too fast to get an immediate stabilization to the dynamic working point of the hysteresis. The simulation show that the \mathcal{C}_π controller gives very interesting

dynamic performances over a wide range of dynamic working points relating to the operating frequency. An optimization algorithm (see §2.3) has been used to adjust the parameters of the \mathcal{C}_π controller in such manner that the shape of the output response y is "as close to" a sine shape⁹.

Remarks This hysteresis model is composed of three subsystems (the first magnetization branch, the increasing and decreasing branches) that switch depending on the value of dH/dt . When $H \ll H_{max}$, the switch between the branches may not be smooth and such "connection" may induce a small transient on y . An illustration is presented in Fig. 27 at a low frequency in comparison with Fig. 24.

The closed-loop has been also tested using a triangular shaped output reference y^* . Figure 28 depicts the magnitude of the magnetic field H and the corresponding (rescaled) magnetic induction B during the control loop process according to the time. The frequency of 5 Hz has been considered as an example holding the parameters of the simulation with the sine reference at 5 Hz.

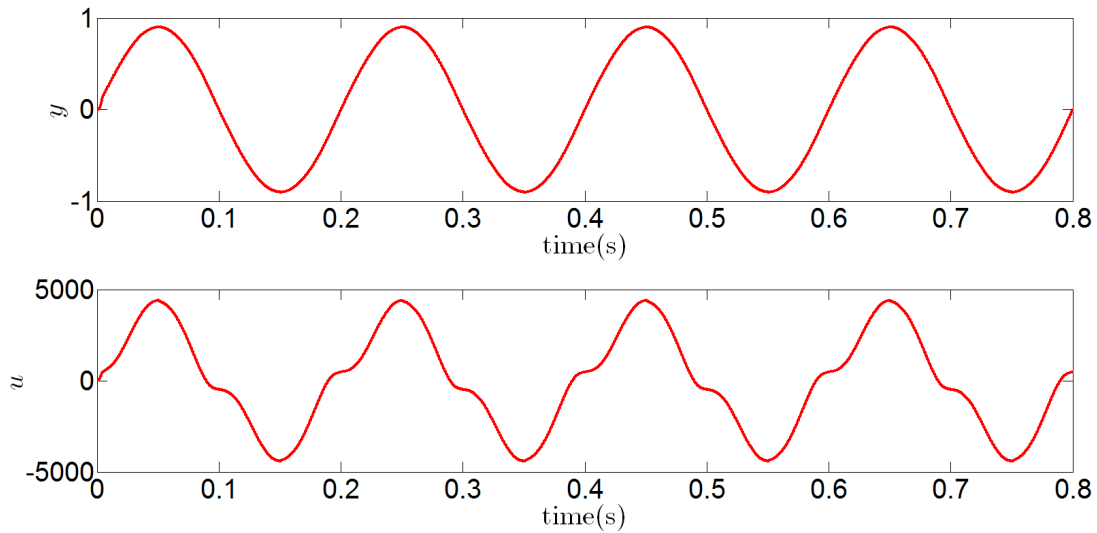


Figure 22: Simulated u and y signals according to the time at 5 Hz.

⁹Remember that the purpose of the optimization procedure is to minimize the tracking error $y^* - y$ in such manner that ideally $y \equiv y^*$ for the particular sine output reference y^* .

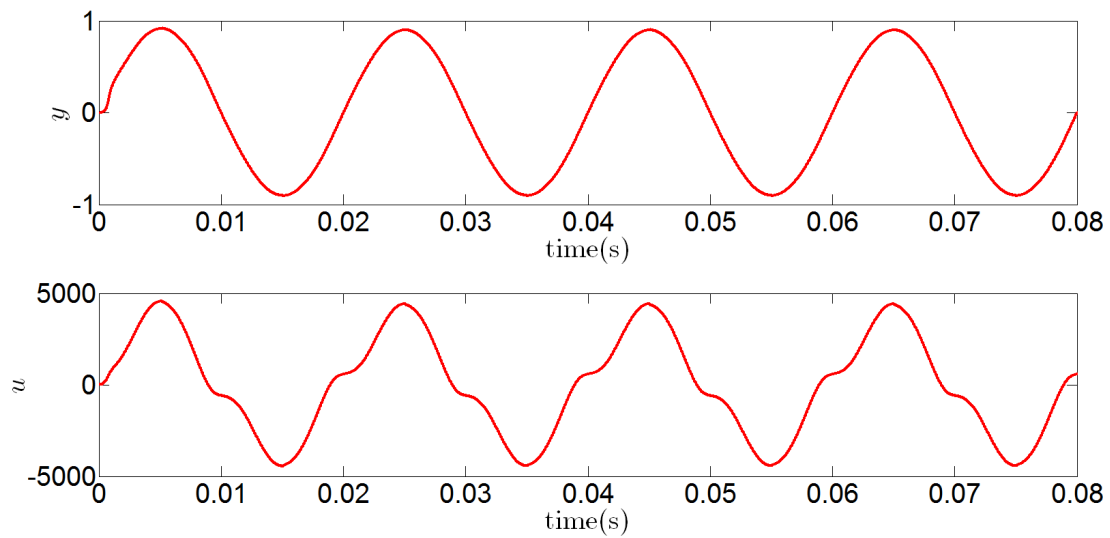


Figure 23: Simulated u and y signals according to the time at 50 Hz.

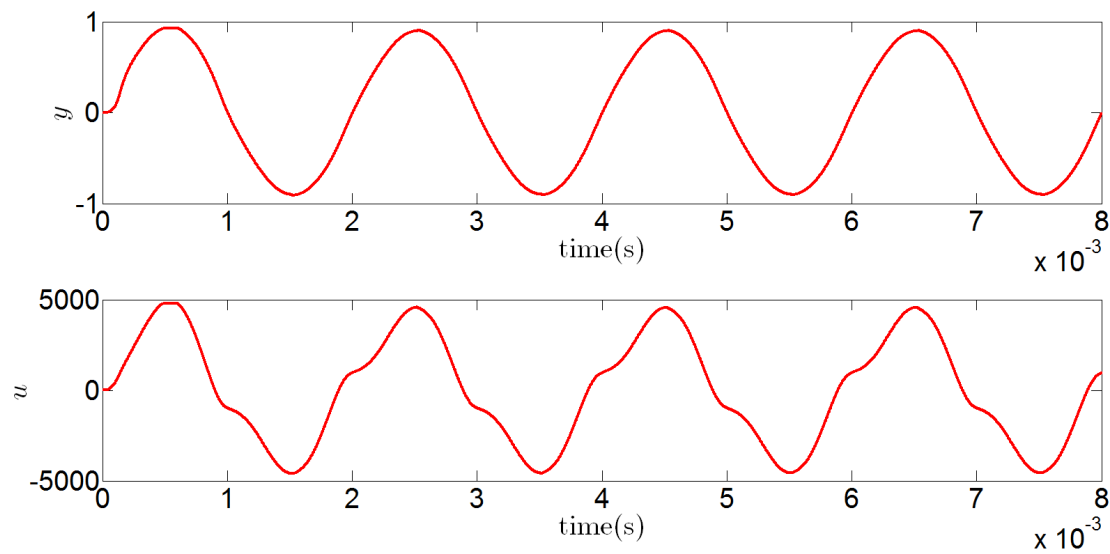


Figure 24: Simulated u and y signals according to the time at 500 Hz.

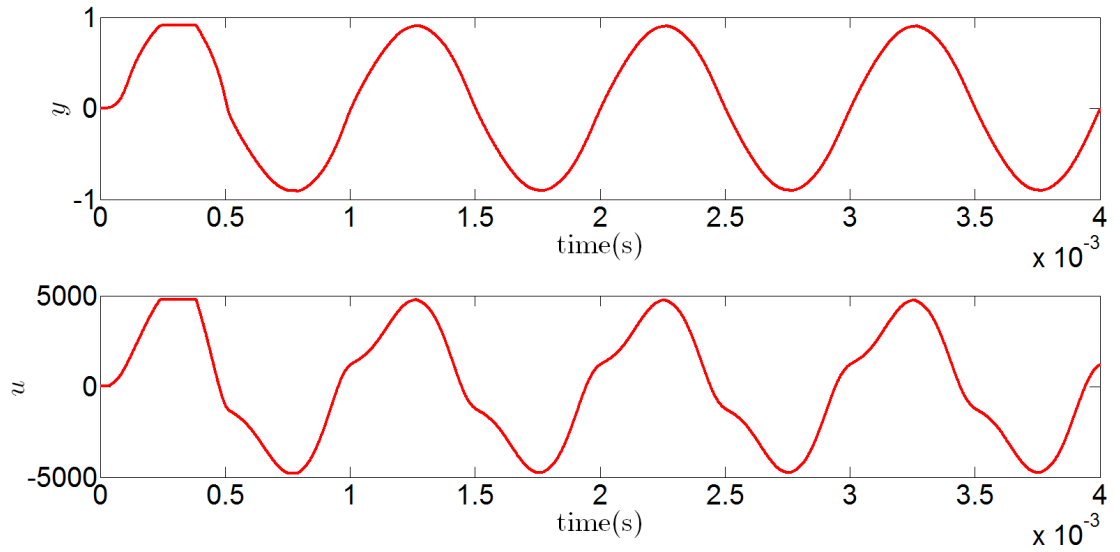


Figure 25: Simulated u and y signals according to the time at 1 kHz.

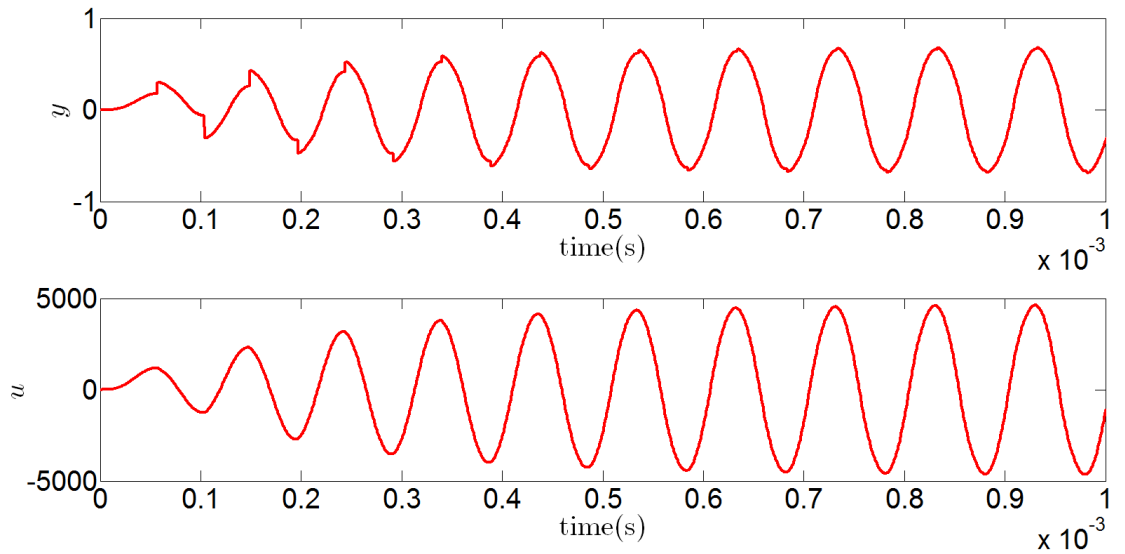


Figure 26: Simulated u and y signals according to the time at 10 kHz.

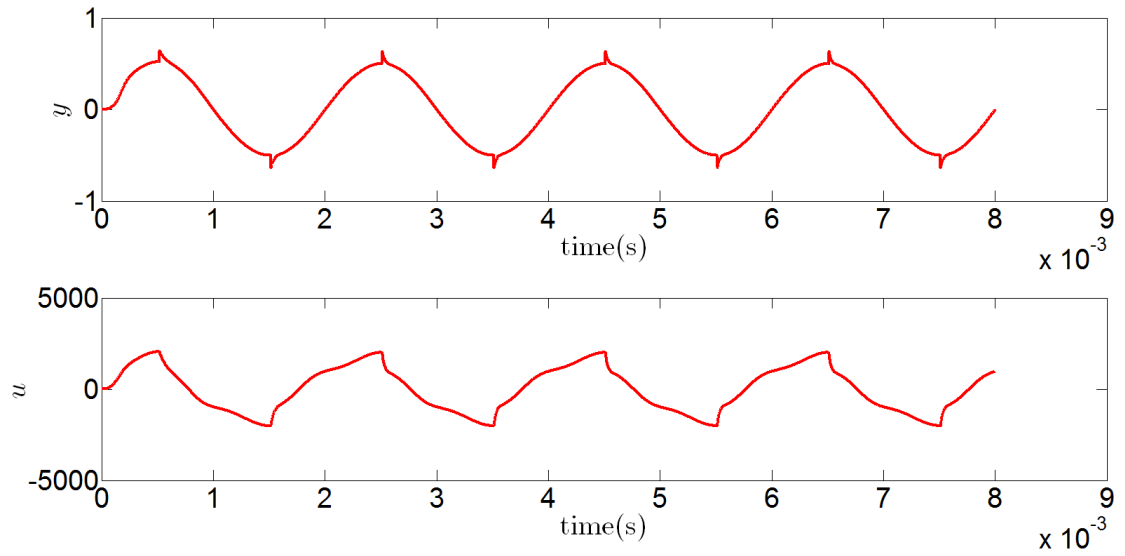


Figure 27: Simulated u and y signals according to the time at 500 Hz ($H \ll H_{max}$).

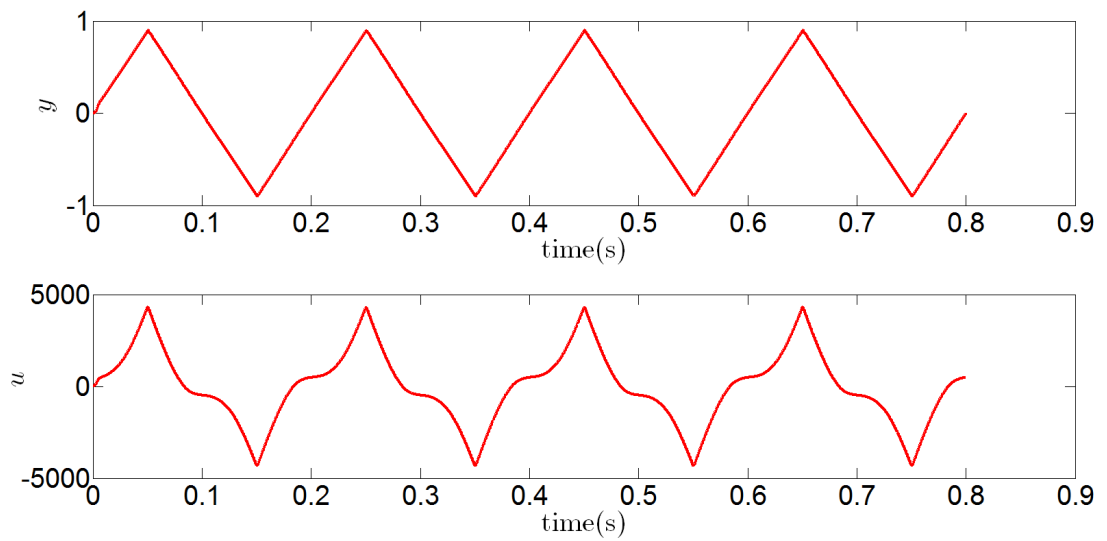


Figure 28: Simulated H and y signals according to the time at 5 Hz.

4 Derivative-free & "extremum-seeking" control

To describe how the PMA could be used as a derivative-free optimization (DFO) algorithm (e.g. [17] [18]) or as an "extremum-seeking" (ES) control scheme (e.g. [19] [20] [21]), we first define each element of the associated control scheme and then, we derive the operating conditions that would allow to minimize nonlinear functions. *We assume that it is possible to derive a control scheme such that the PMA can be used to minimize nonlinear functions.*

4.1 Proposed \mathcal{C}_π control scheme

Definition of the closed loop Consider the control scheme depicted in Fig. 29 where \mathcal{C}_π is the proposed PMA "extremum-seeking" controller. K_{in} and K_{out} are positive real gains. We consider either a static nonlinear function f_{nl}^s (regarding DFO), which does not have any internal dynamical properties, or a nonlinear SISO dynamical system (1) (regarding ES), to minimize. The function Q is a basic first order transfer function.

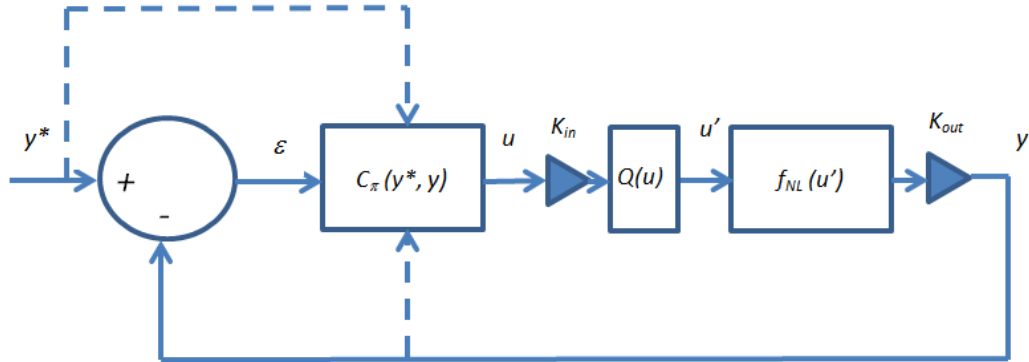


Figure 29: Proposed PMA scheme to minimize a nonlinear function f_{nl} .

Function to control

- Define the f_{nl}^s static function to optimize such that:

$$f_{nl}^s : \begin{matrix} \mathbb{R}^n & \rightarrow & \mathbb{R} \\ u' & \mapsto & y \end{matrix} \quad (17)$$

or consider a nonlinear SISO dynamical system (1).

This function represents the "nonlinear optimization problem". Currently, the assumption $n \leq 2$ is considered and we denote u'_x the input variable for $n = 1$ and (u'_x, u'_y) , the couple of variables for $n = 2$.

- Q is a standard linear transfer function (typically of first order), such that:

$$Q : \frac{du'}{dt} \Big|_k + \gamma u' \Big|_k = u_k \quad \mathbb{R} \rightarrow \mathbb{R} \quad (18)$$

where γ is a time-constant, chosen in such manner that the step response of Q is very fast. As presented in the Fig. 29, Q is associated with f_{nl}^s in order to provide some minimal dynamical properties regarding the system f_{nl}^s to control. Obviously, the Q function is not necessary when f_{nl} is already a dynamical function like (1).

A single \mathcal{C}_π controller drives a single input of f_{nl} (eventually through Q), as presented in Fig. 29. To extend this scheme to multi-input variables ($n > 2$) of f_{nl} , one may consider the use of a \mathcal{C}_π controller per input variable.

4.2 Numerical applications

Since the PMA is designed for nonlinear systems and does not contain any derivatives, it is assumed that the "extremum-seeking" control is possible considering a specific definition of y^* in order to reach and stabilize f_{nl} to its minimum.

Let us assume that the following (eventually constrained) minimization problem (described for a single variable):

$$\min_{x \in \mathbb{R}} f_{nl}(x), \quad (x = u' \text{ identically inside the control scheme}) \quad (19)$$

is equivalent to the control scheme (Fig. 29), for which the output reference y^* "follows" the minimum value of f_{nl} . We denote x_{opt} , the input value that gives the minimum of f_{nl} (resp. (x_{opt}, y_{opt}) in 2D).

Results The following figures show the first results that have been obtained recently. For each case in 1D, are plotted: the difference between two iterations y_k, y_{k-1} and the error between x_{opt} and the evolution of x through the closed-loop. In 2D, the trajectory of the iterations in the "nonlinear landscape" is plotted. In these cases, all the parameters of the \mathcal{C}_π have been set experimentally to give interesting performances but are not optimal (the choice of the y^* function may increase the speed of the convergence). The following numerical cases are studied:

- minimization of a 1D convex function such that:

$$\min_x (x - 30)^2 \quad (20)$$

See Fig. 30.

- minimization of a 1D convex function with a minimum that changes according to the time at an unknown instant t_1 such that:

$$\min_x (x - 30)^2 \xrightarrow{t_1} \min_x (x - 40)^2 \quad (21)$$

See Fig. 31.

- minimization of a 1D non convex function such that:

$$\min_{x,y} 10(1.5 \cos(x) - x) + \exp(x - 5) + 100 \quad \text{subj. to : } y \geq 15x - 60 \quad (22)$$

See Fig. 32.

- minimization of a 2D function such that:

$$\min_{x,y} (x - 7)^2 + 2(x - 7) + (y - 4)^2 - 3(y - 4) \quad (23)$$

with the initial conditions $(x_o, y_o) = (0, 0)$. The minimum point is $(x_{opt}, y_{opt}) = (6, 5.5)$. See Fig. 33.

- minimization of the Rosenbrock function such that: .

$$\min_{xy} (1 - x)^2 + 100(y - x^2)^2 \quad (24)$$

with the initial conditions $(x_o, y_o) = (-10, 10)$. The minimum point is $(x_{opt}, y_{opt}) = (1, 1)$. See Fig. 34.

5 Concluding remarks

We presented how the proposed para-model agent¹⁰, as a model-free and derivative-free based controller, can be used to control nonlinear systems or perform optimization / "extremum-seeking" control. Further investigations include extensive tests and applications to complex systems as well as a complete study of the stability.

Acknowledgement

The author is sincerely grateful to Dr. Edouard Thomas for his strong guidance and his valuable comments that improved this paper. The author is also sincerely grateful to Olivier Ghibaudo, Ph.D. student at G2Elab-CNRS (Grenoble) France, for having worked on the numerical version of the hysteresis model.

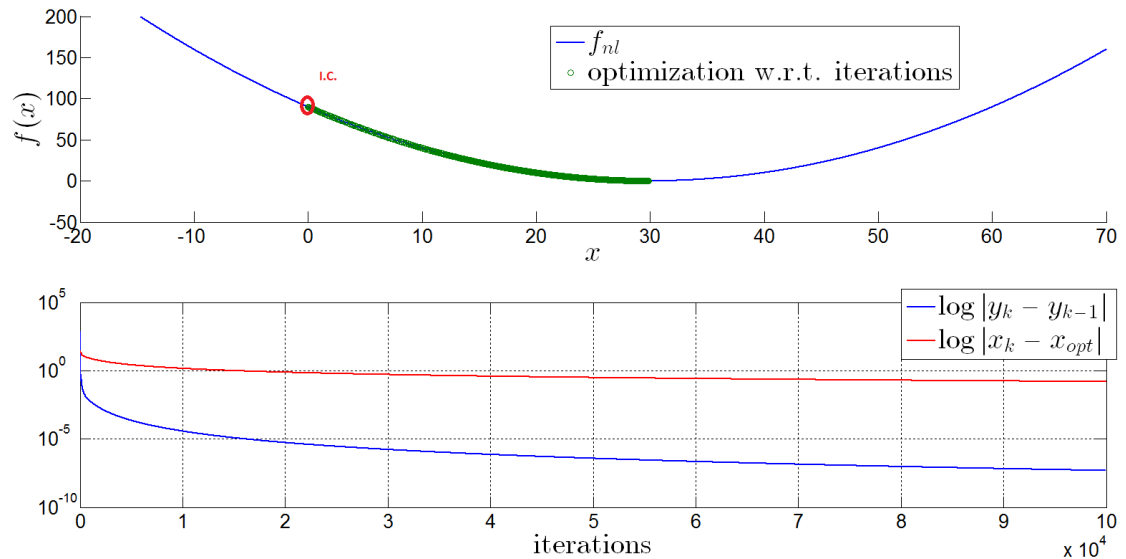


Figure 30: $\min_x (x - 30)^2$ (initial condition in red spot).

¹⁰Why "para-model"? Based on the "model-free" methodology, for which the model is not correlated to the controller in the sense that the controller does not need an explicit definition of the model to be parametrized and can thus rebuild an ultra-local model from measurements, we propose the prefix "para" to highlight the fact that the agent is "in close proximity" to the model of the process that he controls. Although no specific information is needed for the PMA control part, some basic information may be needed to configure properly the PMA and the output reference y^* in the case of extremum-seeking control approach. The stability study is an essential part that should formalize the proposed PMA approach in order to justify theoretically the operating conditions of the \mathcal{C}_π control.

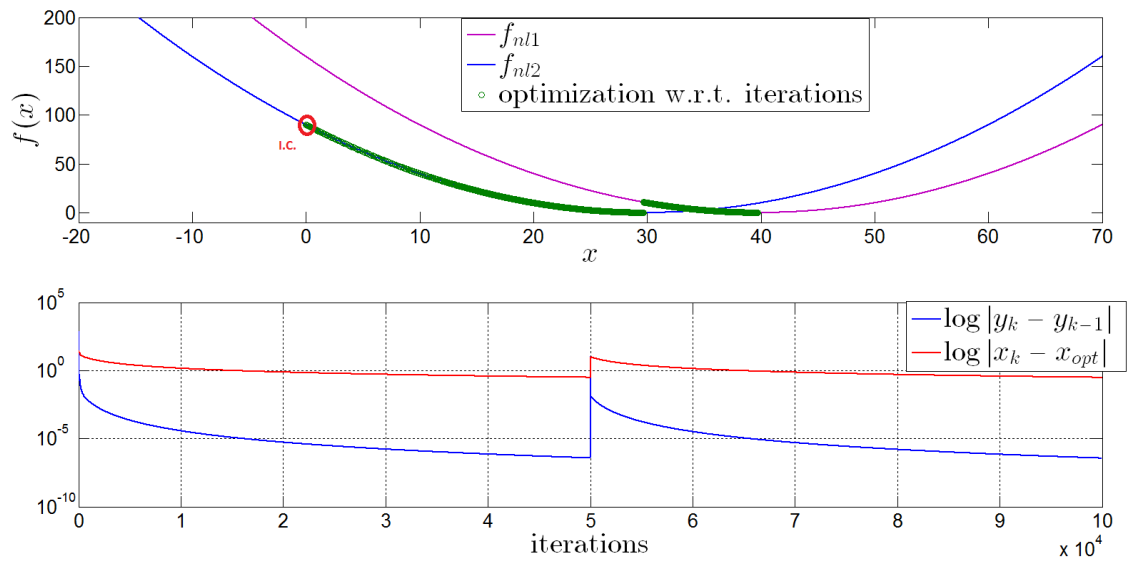


Figure 31: $\min_x f_{nl2} = (x - 30)^2 \xrightarrow{t_1?} \min_x f_{nl1} = (x - 40)^2$ (initial condition in red spot).

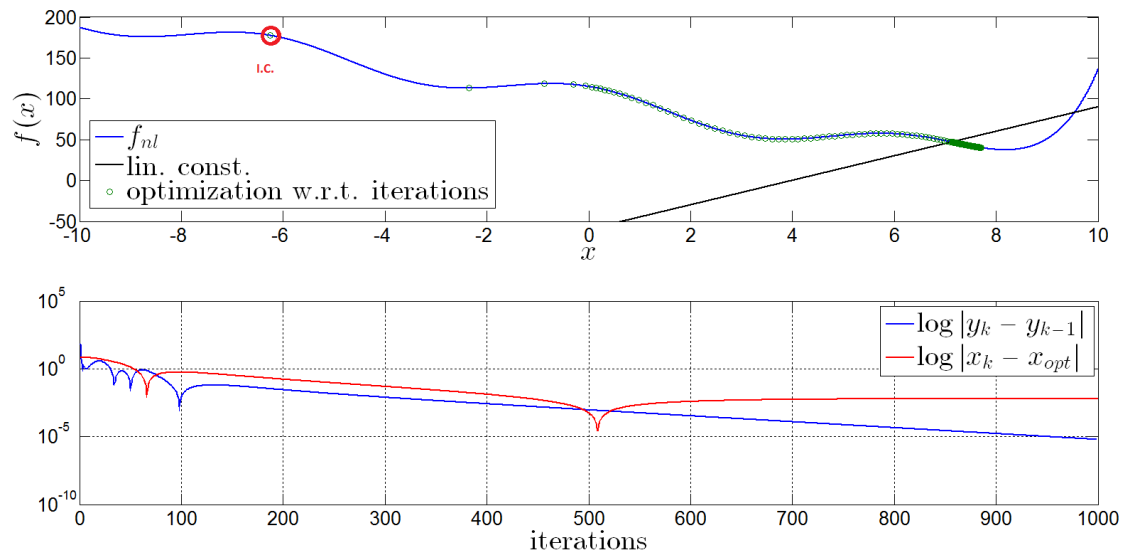


Figure 32: $\min_{x,y} 10(1.5 \cos(x) - x) + \exp(x - 5) + 100$ subj. to : $y \geq 15x - 60$ (initial condition in red spot).

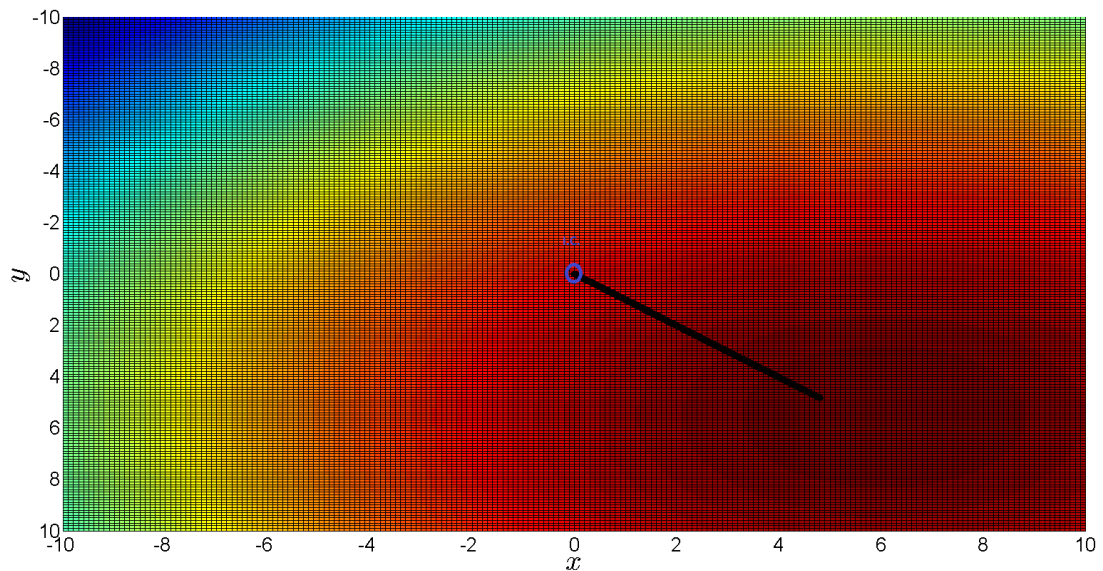


Figure 33: $\min_{x,y} (x - 7)^2 + 2(x - 7) + (y - 4)^2 - 3(y - 4)$ (initial condition in blue spot).

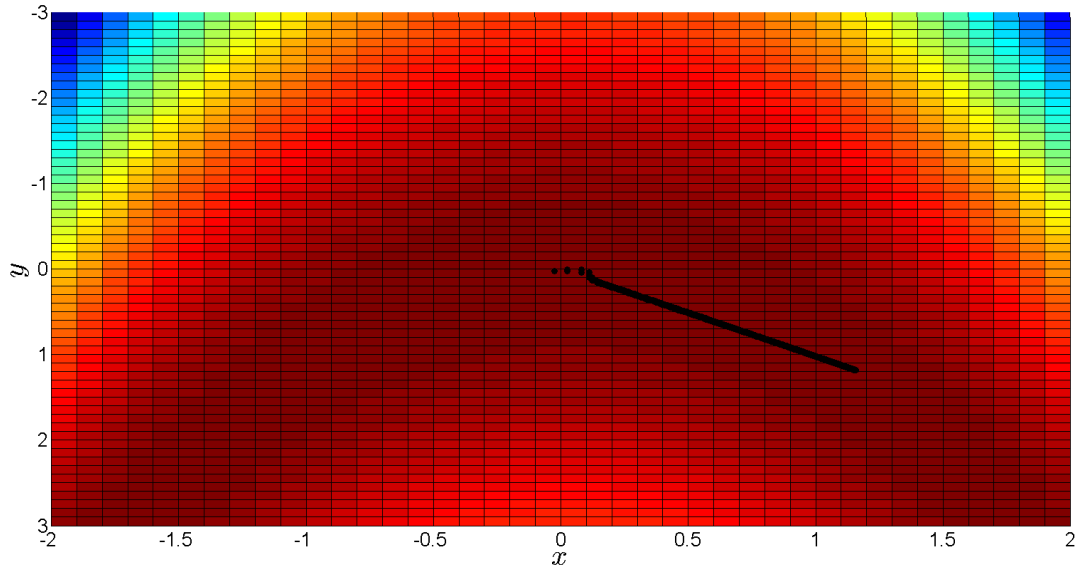


Figure 34: $\min_{xy} (1 - x)^2 + 100(y - x^2)^2$ (initial condition outside the screen).

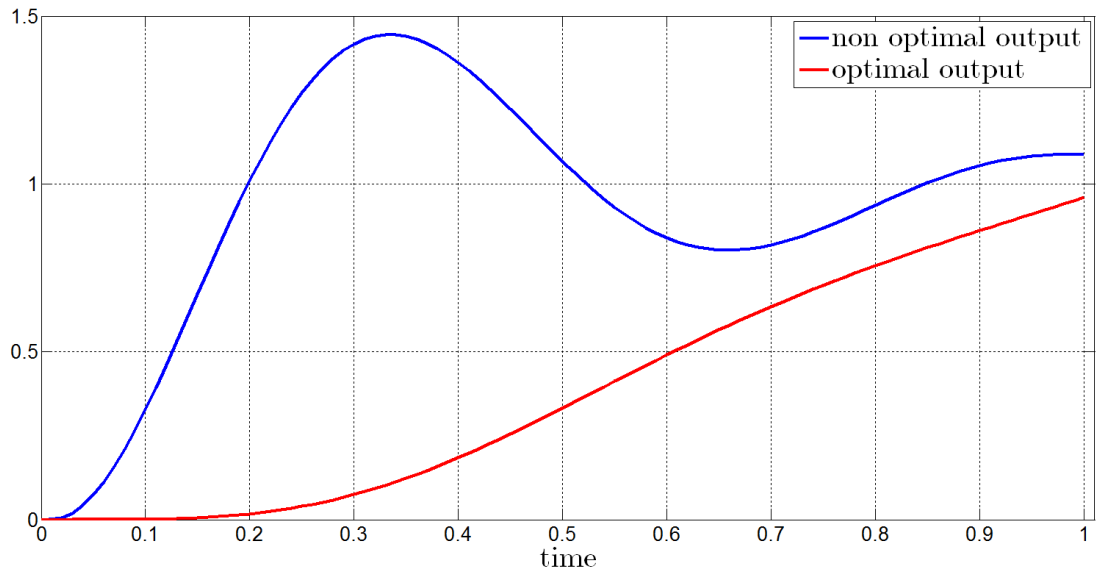


Figure 35: Example of optimal control of f_{nl} .

References

- [1] M. Fliess and C. Join, "Commande sans modèle et commande à modèle restreint", e-STA, vol. 5 (n° 4), pp. 1-23, 2008 (available at <http://hal.inria.fr/inria-00288107/en/>).
- [2] M. Fliess and C. Join, "Model-free control", International Journal of Control, vol. 86, issue 12, pp. 2228-2252, Jul. 2013 (available at <http://arxiv.org/pdf/1305.7085.pdf>).
- [3] K.J. Åström and P.R. Kumar, "Control: A perspective", Automatica, vol. 50, issue 1, pp. 3-43, Jan. 2014 (available at <http://www.sciencedirect.com/science/article/pii/S0005109813005037>).
- [4] K. J. Åström, "Direct methods for nonminimum phase systems", in 19th IEEE Conference on Decision and Control including the Symposium on Adaptive Processes, vol.19, pp.611-615, Dec. 1980.
- [5] A. Isidori, "A tool for semi-global stabilization of uncertain non-minimum-phase nonlinear systems via output feedback", IEEE Transactions on Automatic Control, vol.45, no.10, pp. 1817-1827, Oct. 2000.
- [6] N. Wang, W. Xu and F. Chen, "Adaptive global output feedback stabilisation of some non-minimum phase nonlinear uncertain systems", IET Control Theory & Applications, vol.2, no.2, pp.117-125, Feb. 2008.
- [7] M. Benosman, F. Liao, K.-Y. Lum and J. Liang Wang, "Nonlinear Control Allocation for Non-Minimum Phase Systems", IEEE Transactions on Control Systems Technology, vol.17, no.2, pp.394-404, Mar. 2009.
- [8] R. Gurumoorthy and S.R. Sanders, "Controlling Non-Minimum Phase Nonlinear Systems - The Inverted Pendulum on a Cart Example", 1993 American Control Conference, pp.680-685, June 1993.
- [9] D. Karagiannis, Z.P. Jiang, R. Ortega and A. Astolfi, "Output-feedback stabilization of a class of uncertain non-minimum-phase nonlinear systems", Automatica, vol. 41, Issue 9, September 2005.
- [10] I. Barkana, "Classical and simple adaptive control for nonminimum phase autopilot design", Journal of Guidance Control and Dynamics, vol. 28, Issue: 4, pp. 631-638, 2005.
- [11] L. Michel, "Model-free control of non-minimum phase systems and switched systems", preprint arXiv, 2011 (available at <http://arxiv.org/abs/1106.1697>).

- [12] M. Porcelli and Ph. L. Toint, BFO, "A trainable derivative-free Brute Force Optimizer for nonlinear bound-constrained optimization and equilibrium computations with continuous and discrete variables", *Namur Center for Complex Systems*, In Support, Tech. Reports, no. naXys-06-2015, Belgium, Jul. 2015 (available at http://www.optimization-online.org/DB_FILE/2015/07/4986.pdf).
- [13] L. Michel, C. Join, M. Fliess, P. Sicard and A. Chriti, "Model-free control of dc/dc converter", in 2010 IEEE 12th Workshop on Control and Modeling for Power Electronics, pp.1-8, June 2010 (available at <http://hal.inria.fr/inria-00495776/>).
- [14] M. Barão and J.M. Lemos, "Nonlinear control of HIV-1 infection with a singular perturbation model", *Biomedical Signal Processing and Control*, vol. 2, issue 3, pp. 248-257, July 2007.
- [15] I. K. Craig, X. Xia and J. W. Venter, "Introducing HIV/AIDS education into the electrical engineering curriculum at the University of Pretoria," *IEEE Transactions on Education*, vol. 47, no. 1, pp. 65-73, Feb. 2004.
- [16] D. C. Jiles and D. L. Atherton, "Theory of ferromagnetic hysteresis", *J. Appl. Phys.* 55, 2115 (1984).
- [17] A.R. Conn, K. Scheinberg and L.N. Vicente, "Introduction to Derivative-Free Optimization", SIAM Publications (Philadelphia), 2009.
- [18] L. M. Rios and N. V. Sahinidis, "Derivative-free optimization: a review of algorithms and comparison of software implementations", *Journal of Global Optimization*, Volume 56, Issue 3, pp 1247-1293, Jul. 2013 (available at <http://link.springer.com/article/10.1007/s10898-012-9951-y>).
- [19] K. B. Ariyur and M. Krstic, "Real-Time Optimization by Extremum-Seeking Control", Wiley, 2003.
- [20] Y. Tan, W.H. Moase, C. Manzie, D. Nesic and I.M.Y. Mareels, "Extremum Seeking From 1922 To 2010", 2010 29th Chinese Control Conference (CCC), pp.14,26, 29-31 July 2010.
- [21] A. O. Vweza, K. To Chong and D. J. Lee, "Gradient-free numerical optimization-based extremum seeking control for multiagent systems", *International Journal of Control, Automation and Systems*, May 2015.